NAVAL POSTGRADUATE SCHOOL

MONTEREY, CALIFORNIA

THESIS

POWER TRANSFER EFFICIENCY OF MUTUALLY COUPLED COILS IN AN ALUMINUM AUV HULL

by

James M. Cena

December 2013

Thesis Co-Advisors: David Jenn
Alexander L. Julian

Approved for public release; distribution is unlimited

THIS PAGE INTENTIONALLY LEFT BLANK

REPORT DOCUMENTATION PAGE			*Form Approved OMB No. 0704-0188*
Public reporting burden for this collection of information is estimated to average 1 hour per response, including the time for reviewing instruction, searching existing data sources, gathering and maintaining the data needed, and completing and reviewing the collection of information. Send comments regarding this burden estimate or any other aspect of this collection of information, including suggestions for reducing this burden, to Washington headquarters Services, Directorate for Information Operations and Reports, 1215 Jefferson Davis Highway, Suite 1204, Arlington, VA 22202-4302, and to the Office of Management and Budget, Paperwork Reduction Project (0704-0188) Washington DC 20503.			
1. AGENCY USE ONLY ***(Leave blank)***	**2. REPORT DATE** December 2013	**3. REPORT TYPE AND DATES COVERED** Master's Thesis	
4. TITLE AND SUBTITLE POWER TRANSFER EFFICIENCY OF MUTUALLY COUPLED COILS IN AN ALUMINUM AUV HULL		**5. FUNDING NUMBERS**	
6. AUTHOR(S) James M. Cena			
7. PERFORMING ORGANIZATION NAME(S) AND ADDRESS(ES) Naval Postgraduate School Monterey, CA 93943-5000		**8. PERFORMING ORGANIZATION REPORT NUMBER**	
9. SPONSORING /MONITORING AGENCY NAME(S) AND ADDRESS(ES) N/A		**10. SPONSORING/MONITORING AGENCY REPORT NUMBER**	
11. SUPPLEMENTARY NOTES The views expressed in this thesis are those of the author and do not reflect the official policy or position of the Department of Defense or the U.S. Government. IRB Protocol number ____N/A____.			
12a. DISTRIBUTION / AVAILABILITY STATEMENT Approved for public release; distribution is unlimited		**12b. DISTRIBUTION CODE** A	

13. ABSTRACT (maximum 200 words)

To charge the United States Navy's Remote Environmental Measuring Units (REMUS) autonomous undersea vehicle (AUV) in situ requires the REMUS to mate with a docking station. There are two problems with this docking station. The docking system requires the REMUS to make electrical contact with the dock, which can lead to electrical shorting in an undersea environment. The dock is also designed to fit a single type of AUV. AUVs of different sizes require a new docking system. A different means of power transfer is required that can be used in a universal docking station.

An inductive power transfer (IPT) system can be used in a universal docking station. In this report, we calculated the power transfer efficiency of an IPT system operating at 100 kHz using circular coils. These calculated results were then compared to three sets of measured efficiency data: an IPT system without ferrite tiles; an IPT system with the receiving coil attached to ferrite tiles; and an IPT system with the receiving coil/ferrite tile combination placed inside an aluminum AUV hull. Efficiency was poor, less than 10 percent with an air gap of 55 mm, when the receiving coil was placed inside the aluminum hull.

14. SUBJECT TERMS Wireless power transfer, inductive power transfer, mutually coupled coils, autonomous undersea vehicle (AUV), power transfer efficiency, quality Factor (*Q*), coupling coefficient (*k*), two coil system	**15. NUMBER OF PAGES** 93
	16. PRICE CODE

17. SECURITY CLASSIFICATION OF REPORT	**18. SECURITY CLASSIFICATION OF THIS PAGE**	**19. SECURITY CLASSIFICATION OF ABSTRACT**	**20. LIMITATION OF ABSTRACT**
Unclassified	Unclassified	Unclassified	UU

NSN 7540-01-280-5500 Standard Form 298 (Rev. 2-89)
Prescribed by ANSI Std. 239-18

THIS PAGE INTENTIONALLY LEFT BLANK

Approved for public release; distribution is unlimited

POWER TRANSFER EFFICIENCY OF MUTUALLY COUPLED COILS IN AN ALUMINUM AUV HULL

James M. Cena
Lieutenant Commander, United States Navy
B.S., University of San Diego, 2001

Submitted in partial fulfillment of the
requirements for the degree of

MASTER OF SCIENCE IN ELECTRICAL ENGINEERING

from the

NAVAL POSTGRADUATE SCHOOL
December 2013

Author: James M. Cena

Approved by: David Jenn
Thesis Co-Advisor

Alexander L. Julian
Thesis Co-Advisor

R. Clark Robertson
Chair, Department of Electrical and Computer Engineering

THIS PAGE INTENTIONALLY LEFT BLANK

ABSTRACT

To charge the United States Navy's Remote Environmental Measuring Units (REMUS) autonomous undersea vehicle (AUV) in situ requires the REMUS to mate with a docking station. There are two problems with this docking station. The docking system requires the REMUS to make electrical contact with the dock, which can lead to electrical shorting in an undersea environment. The dock is also designed to fit a single type of AUV. AUVs of different sizes require a new docking system. A different means of power transfer is required that can be used in a universal docking station.

An inductive power transfer (IPT) system can be used in a universal docking station. In this report, we calculated the power transfer efficiency of an IPT system operating at 100 kHz using circular coils. These calculated results were then compared to three sets of measured efficiency data: an IPT system without ferrite tiles; an IPT system with the receiving coil attached to ferrite tiles; and an IPT system with the receiving coil/ferrite tile combination placed inside an aluminum AUV hull. Efficiency was poor, less than 10 percent with an air gap of 55 mm, when the receiving coil was placed inside the aluminum hull.

THIS PAGE INTENTIONALLY LEFT BLANK

TABLE OF CONTENTS

LIST OF FIGURES

LIST OF TABLES

THIS PAGE INTENTIONALLY LEFT BLANK

LIST OF ACRONYMS AND ABBREVIATIONS

USN	United States Navy
REMUS	remote environmental measuring units
AUV	autonomous underwater vehicle
WHOI	Woods Hole Oceanographic Institute
IPT	inductive power transfer
WPT	wireless power transfer
ADS	advanced design system
SSC	Space and Naval Warfare System Center
AWG	American Wire Gauge
UHF	ultra high frequency
VNA	Vector Network Analyzer

THIS PAGE INTENTIONALLY LEFT BLANK

EXECUTIVE SUMMARY

The United States Navy (USN) is working on a new way to recharge the Remote Environmental Measuring Units (REMUS) autonomous underwater vehicle (AUV) in situ. The current method of recharging the REMUS requires the REMUS to perform an underwater precision docking with a standalone docking platform. This method of recharging the REMUS is limited to this specific class of REMUS AUV, and a more robust design is needed to accommodate the different types of AUVs in the USN inventory. A photograph of the REMUS AUV mated with its docking station is shown in Figure 1. To satisfy the need of recharging different types of AUVs and to eliminate the need for electrical contacts, a new docking station is needed and a new common method of power transfer is required.

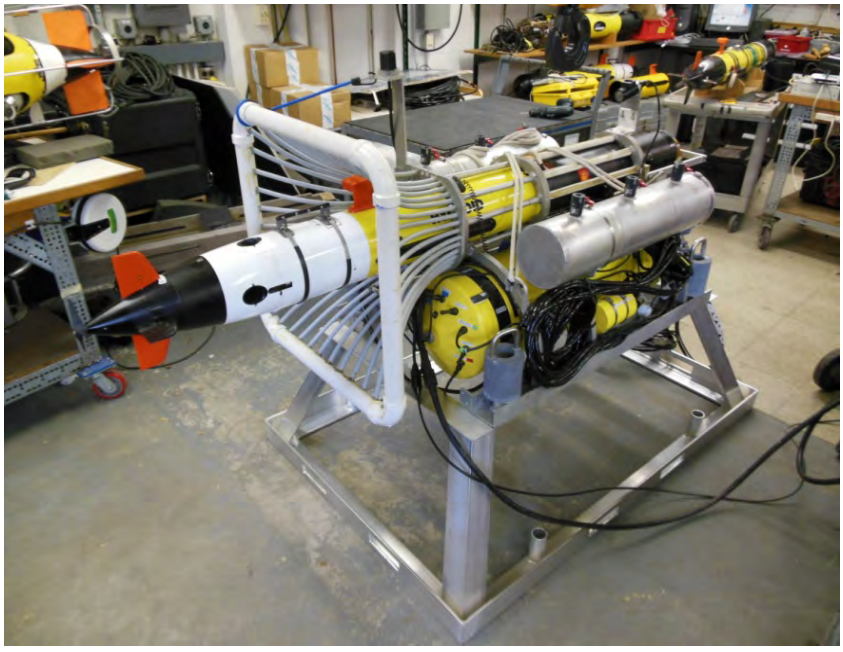

Figure 1. The Naval Postgraduate School (NPS) REMUS in a Woods Hole Oceanographic Institute (WHOI) dock for lab testing (from [1]).

To understand why a new power transfer method is needed, we first need to know how a REMUS AUV currently recharges its batteries in situ. To recharge its batteries, a

REMUS must approach and enter into proper alignment with the docking station. Once inside the docking station, the REMUS must be aligned to the dock to allow for the nose cone of the REMUS to engage the docking station power and data contacts [2]. The REMUS docking station was designed to help prevent seawater interference between the REMUS and docking station [2]. Anytime electrical contacts are exposed to seawater there is a possibility of shorting and corrosion of the electrical contacts. This leads to damaged equipment and poor power transfer efficiency [3].

Another shortfall in using this docking platform is that it was designed to support only one specific class of REMUS AUV. An AUV with a larger or smaller hull diameter cannot use this platform for charging. Therefore, to support the USN's various AUVs, the USN will have to purchase numerous docking stations of varying sizes. To eliminate the need for physical docking contacts for battery charging and avoid the need to purchase different docking platforms, a flexible noncontact method of battery charging is needed for the REMUS.

Inductive power transfer (IPT) is a wireless power transfer (WPT) method that uses two coils and near-field magnetic coupling for power transfer in a system. IPT is currently being used by electric buses, trains, and cars as a method for wirelessly charging these vehicles through an air gap [4]. The benefit of using IPT is that it allows for efficient power transfer (>70 percent with a 40 mm air gap) with a high degree of misalignment between the two coils [5]. IPT eliminates the need for physical contacts between the AUV and a docking station and provides a safer way of battery charging underwater. Also, with a proper docking station design, IPT can be adapted to charge a variety of different AUV types as shown in Figure 2. The focus of this research is on determining the power transfer efficiency of a series-series compensated IPT system for different air gaps. This research is different from other work in this area because power transfer efficiency is measured when the IPT receiving coil is placed inside an aluminum AUV hull.

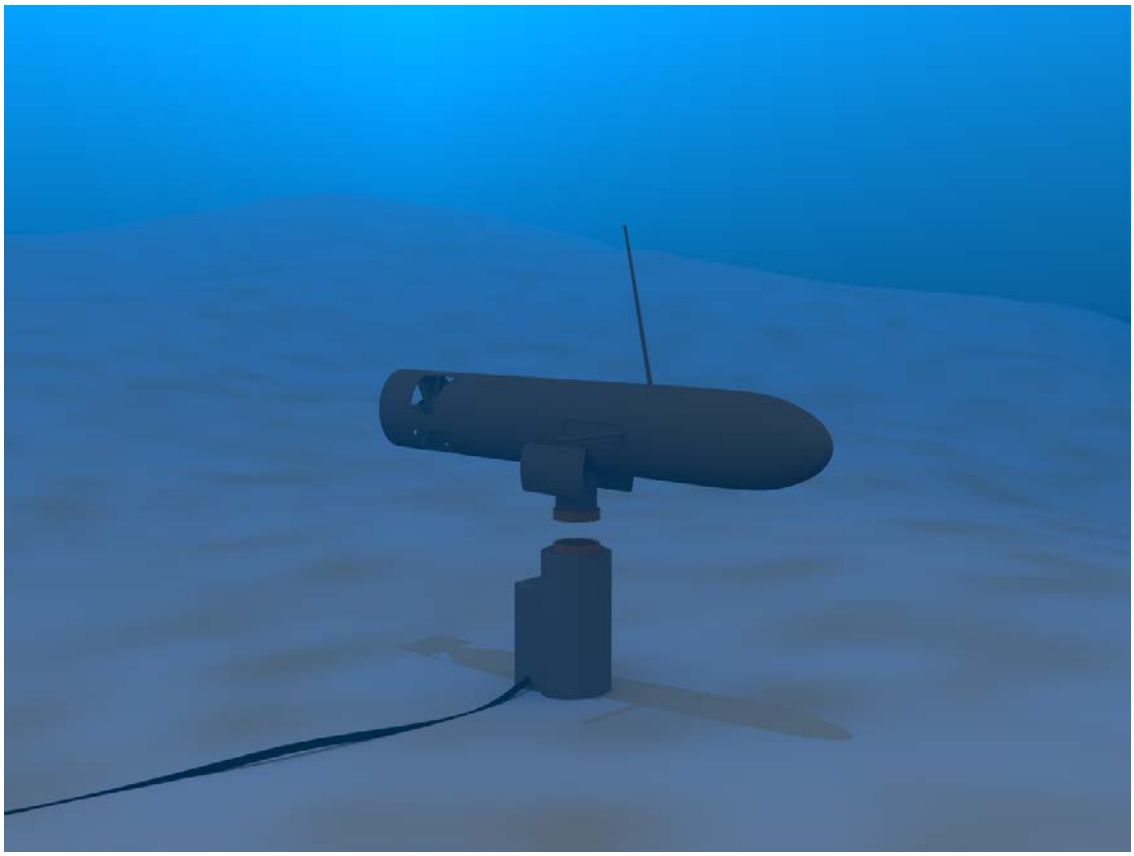

Figure 2 Nominal IPT docking system designed for charging different hull diameter AUVs (from [6]).

The objective of this thesis research is to analytically and quantitatively determine the power transfer efficiency of two circular magnetically coupled coils at various air gaps. Power transfer efficiency measurements of the series-series compensated system, as shown in Figure 3, were performed with and without ferrite tiles. The measured efficiency results were then compared to the calculated efficiencies for further analysis. Finally, power transfer efficiency was measured when the receiving coil and ferrite tiles were placed inside an aluminum AUV hull.

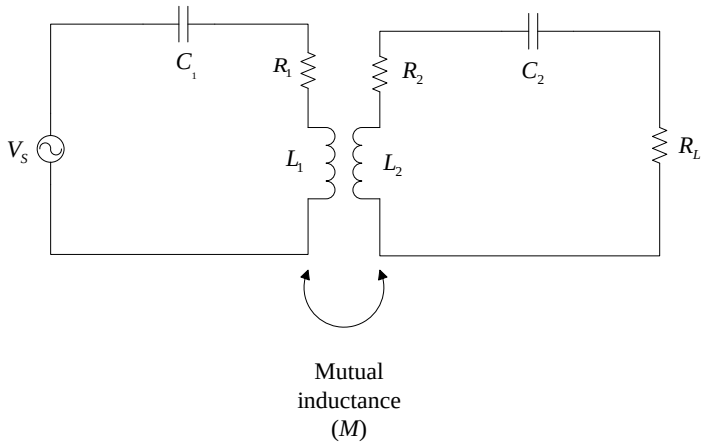

Figure 3. Simplified circuit model for a series-series compensated topology for a loosely coupled IPT system.

The method of power transfer in an IPT system can be illustrated with two coils placed in close proximity to each other, as shown in Figure 4. Using Faraday's law it can be shown that a time-varying current in coil 1 I_1 induces a time-varying magnetic flux Φ_{21} in coil 2. This time-varying magnetic flux in coil 2 in turn induces a voltage in coil 2. This method of using linked magnetic flux between coil 1 and coil 2 is how IPT transfers power wirelessly.

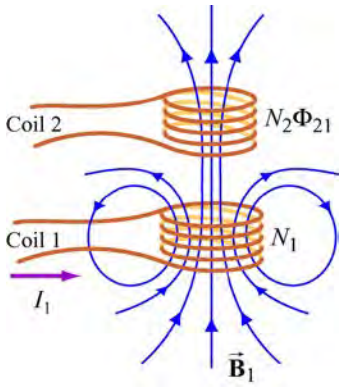

Figure 4. Alternating current in coil 1 produces a time-varying magnetic flux in coil 2 (from [7]).

Using basic electrical equations with Figure 3, we can derive the system's power transfer efficiency η as

$$\eta = \frac{R_L(\omega_0 M)^2}{R_1(R_2 + R_L)^2 + (\omega_0 M)^2(R_2 + R_L)}, \quad (1)$$

where R_1 is the internal resistance of the transmitting coil, R_2 is the internal resistance of the receiving coil, R_L is the load resistance, M is the mutual inductance between the transmitting and receiving coils and ω_0 is the angular frequency of the IPT system.

Based on Eq. (1), we can show that there is an ideal matched load resistance for a given distance between the transmitting and receiving coils. To determine the ideal matched load resistance, we need to differentiate η with respect to R_L, set the result equal to zero, and solve for R_L. The resulting $R_{L,matched}$ can be expressed as [8]

$$R_{L,matched} = \sqrt{R_2^2 + (\omega M)^2 \frac{R_2}{R_1}}. \quad (2)$$

For our IPT system, the transmitting coil (coil 1) and receiving coil (coil 2) were connected following the circuit model shown in Figure 3. The power supply used for the system was an Agilent 33220A function generator connected in series with a Krohn-Hite 50 Watt amplifier. The capacitances were provided by two capacitance substituter boxes. An IET labs resistance substituter was used for the load resistance. The coils were attached to wooden stands using zip ties for support and ease of movement. The entire system setup is shown in Figure 5. The coil on the left in the photo is transmitting. The coil on the right is receiving and is placed inside an aluminum AUV hull. Not shown in Figure 5 are the ferrite tiles placed behind the receiving coil.

Figure 5 Setup of the transmitting coil and receiving coil with ferrite tiles placed inside an AUV hull.

Voltage measurements were taken across the transmitting coil using a Tektronix TDS 3032B oscilloscope. The current measurements were taken in series with the transmitting coil using a Tektronix TCPA 300 Amplifier and a TCP 305A current probe. The phase angle between the voltage and current waveforms was measured using the oscilloscope and converting the time between the voltage and current zero crossings to a corresponding phase angle. The load voltage and current were taken at the resistance substituter box using the oscilloscope and current probe. The distance between the coils was measured from the outer edge of the transmitting coil to the outer edge of the receiving coil. Due to the zip ties and the thickness of the urethane material, the smallest distance between the coils attainable was 16 mm. The distance between the coils was varied from 16 mm to 150 mm.

At each distance increment the load resistance was changed in accordance with $R_{L,matched}$. After the load resistance was changed, the transmitted voltage, current and phase angle between the voltage and current was measured. The transmitted power was determined using

$$P_t = V_{rms} I_{rms} \cos\theta, \tag{3}$$

where P_t, V_{rms}, I_{rms}, and θ are the power, rms voltage, rms current, and phase angle, respectively, measured at the transmitting coil. The power delivered to the load was determined using

$$P_L = V_L I_L, \tag{4}$$

where P_L is the power delivered to the load, V_L and I_L are the load voltage and load current, respectively. Power transfer efficiency of the system was determined using Eq. (1).

Using the measurement procedure previously discussed, we plotted three cases of efficiency versus air gap distance data as shown in Figure 6. The first set of data was for the IPT system without the ferrite tiles behind the receiving coil. The second set of data was for the IPT system with ferrite tiles placed behind the receiving coil. The final set of data was for the IPT system with the receiving coil and ferrite tiles placed inside an aluminum AUV hull. From inspection of Figure 6, it is seen that the ferrite plates increased the efficiency of the IPT system when compared to the IPT system without ferrite tiles. It was also shown that system efficiency was affected by the aluminum hull. Since the receiving coil was inside the aluminum hull, the aluminum hull acted as an attenuator due to eddy currents generated on the hull. Since the receiving coil was not fully encased by the aluminum hull, some free space magnetic coupling did occur between the coils but became weaker as distance between the coils increased. This caused lower system efficiency when compared to the other plotted data.

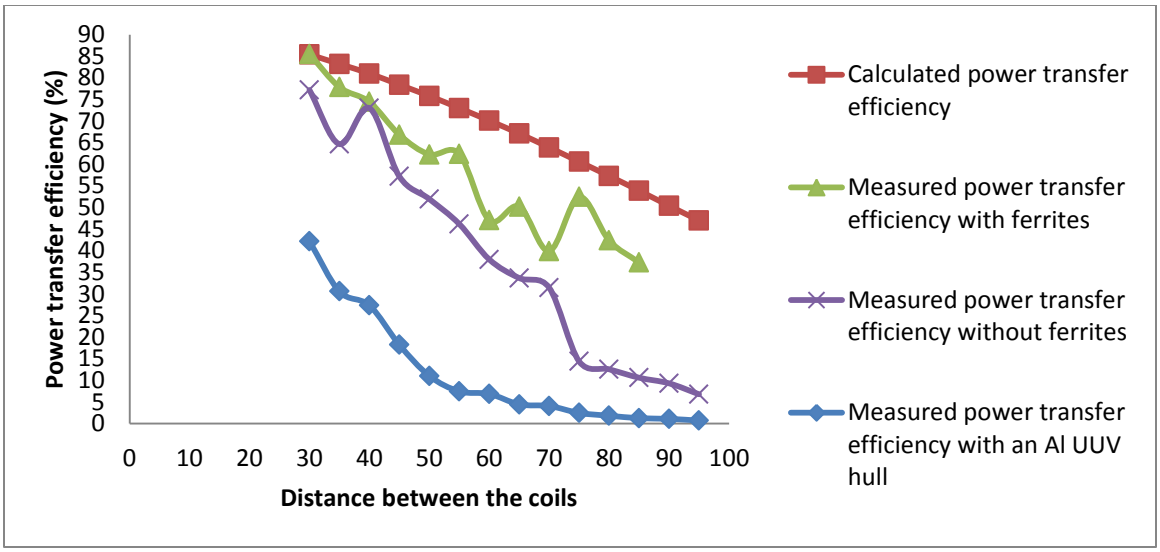

Figure 6. The measured and calculated power transfer efficiency of the IPT system.

System efficiency dropped from 85.5 percent without the aluminum hull to 42.2 percent with the aluminum hull. As is, the drop in efficiency makes using IPT unacceptable to meet the needs of the USN, but there exists methods to increase system efficiency. Such methods are: change the compensation topology; increase system frequency; increase the number of coils; change the hull material surrounding the receiving coil; increase the distance the receiving coil extends past the AUV hull; improve the coil's quality factor; improve the coil's coupling coefficient; and change the material of the coils.

In conclusion, IPT can be a viable method to charge an AUV in situ, as shown by the data plotted in Figure 6, but some changes to this IPT system are needed to increase power transfer efficiency. By using some of the methods discussed previously, we can raise the efficiency of an IPT system and demonstrate that IPT is a viable option to charge a REMUS AUV. We can then leverage this information to create a single docking station that could accommodate all types of AUV hulls. The shift from purchasing multiple docking stations to a single docking station will save the USN money. We recommend continuing work in this research area.

LIST OF REFERENCES

[1] Woods Hole Oceanographic Institution (WHOI), "AUV docking station integration with NPS Monterey Inner Shelf Observatory (MISO)," SPAWAR, San Diego, CA, Status Report Jun. 2013.

[2] R. Stokey, M. Purcell, N. Forrester, T. Austin, R. Goldsborough, B. Allen and C. Alt, "A docking system for REMUS, an autonomous underwater vehicle," in IEEE Conf. OCEANS, Halifax, Canada, pp. 1132–1136, 1997.

[3] V. Bana G. Anderson, L. Xu, D. Rodriguez, A. Phipps and J. Rockway, "Characterization of coupled coils in seawater for wireless power transfer," SPAWAR, San Diego, CA, Tech. Rep. 2026, 2013.

[4] N. Shinohara, "Power without wires," *IEEE Microwave*, vol. 12, no. 7, pp. S64–S73, Dec. 2011.

[5] J. Sallan, A. Llombart and J. Sanz, "Optimal design of ICPT systems applied to electric vehicle battery charge," *IEEE Trans. Ind. Electron.*, vol. 56, no. 6, pp. 2140–2149, Jun. 2009.

[6] V. Bana, private communication, August 2013.

[7] F. Ulaby, "Maxwell's equations for time-varying fields," in Fundamentals of applied electromagnetics, 5th ed. Upper Saddle River: Pearson Prentice Hall, ch. 6, pp. 255–270, 2007.

[8] J. Garnica, J. Casanova and J. Lin, "High efficiency midrange wireless power transfer system," in IEEE MTT-S Int. Microwave Workshop Series on Innovative Wireless Power Transmission: Technologies, Systems, and Applications, Kyoto, pp. 73–76, 2011.

THIS PAGE INTENTIONALLY LEFT BLANK

ACKNOWLEDGMENTS

I would like to thank the following people for their help during this thesis work. Your advice, support and guidance mean a lot to me and were critical in the successful completion of this work:

David Jenn, Naval Postgraduate School,

Alexander Julian, Naval Postgraduate School,

Robert Broadston, Naval Postgraduate School,

Viktor Bana, SSC Pacific, and

My family: Melanie, Deanna and Caitlyn.

THIS PAGE INTENTIONALLY LEFT BLANK

I. INTRODUCTION

A. INDUCTIVE POWER TRANSFER FOR UNDERSEA UNMANNED VEHICLES

The United States Navy (USN) is working on a new way to recharge the Remote Environmental Measuring Units (REMUS) autonomous underwater vehicle (AUV) in situ. The current method of recharging the REMUS requires the REMUS to perform an underwater precision docking with a standalone docking platform to mate with electrical contacts. This method of recharging the REMUS is limited to this specific class of REMUS AUVs, and a more robust design is needed to accommodate the different types of AUVs in the USN inventory. A photograph of the REMUS AUV mated with its docking station is shown in Figure 1. To satisfy the need of recharging different types of AUVs and to eliminate the need for electrical contacts, a new docking station is needed and a new common method of power transfer is required.

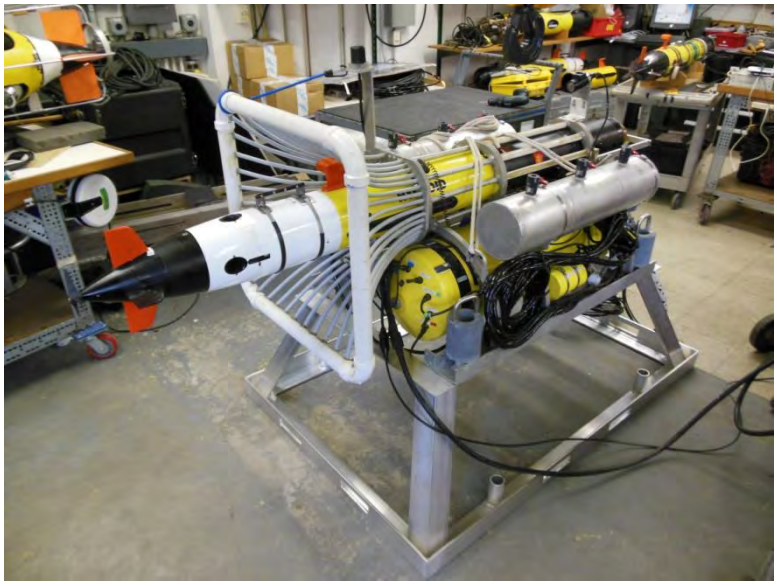

Figure 1. The Naval Postgraduate School (NPS) REMUS in a Woods Hole Oceanographic Institute (WHOI) dock for lab testing (from [1]).

To understand why a new power transfer method is needed we first need to know how a REMUS AUV currently recharges its batteries in situ. To recharge its batteries a

REMUS must approach and enter into proper alignment with the docking station. Once inside the docking station, the REMUS must be aligned to the dock to allow for the nose cone of the REMUS to engage the docking station power and data contacts [2]. The REMUS docking station was designed to help prevent seawater interference between the REMUS and docking station [2]. Anytime electrical contacts are exposed to seawater there is a possibility of shorting and corrosion of the electrical contacts. This leads to damaged equipment and poor power transfer efficiency [3].

Another shortfall in using this docking platform is that it was designed to support only one specific class of REMUS AUV. An AUV with a larger or smaller hull diameter would not be able to use this platform for charging. To support the USN's various AUVs, the USN would have to purchase numerous docking stations of varying sizes. To eliminate the need for physical docking contacts for battery charging and avoid the need to create different docking platforms, a flexible noncontact method of battery charging is needed for the REMUS.

Inductive power transfer (IPT) is a wireless power transfer (WPT) method that uses two coils and near-field magnetic coupling for power transfer in a system. IPT is currently being used by electric buses, trains, and cars as a method for wireless charging these vehicles through an air gap [4]. The benefit of using IPT is that it allows for efficient power transfer (>70 percent with a 40 mm air gap) with a high degree of misalignment between the two coils [5]. IPT eliminates the need for physical contacts between the AUV and a docking station and provides a safer way of battery charging underwater. Also, with a proper docking station design, IPT can be adapted to charge a variety of different AUV types as shown in Figure 2. The focus of this research is on determining the power transfer efficiency of a series-series compensated IPT system for different air gaps. This research is different from other work in this area because power transfer efficiency is measured when the IPT receiving coil is placed inside an aluminum AUV hull.

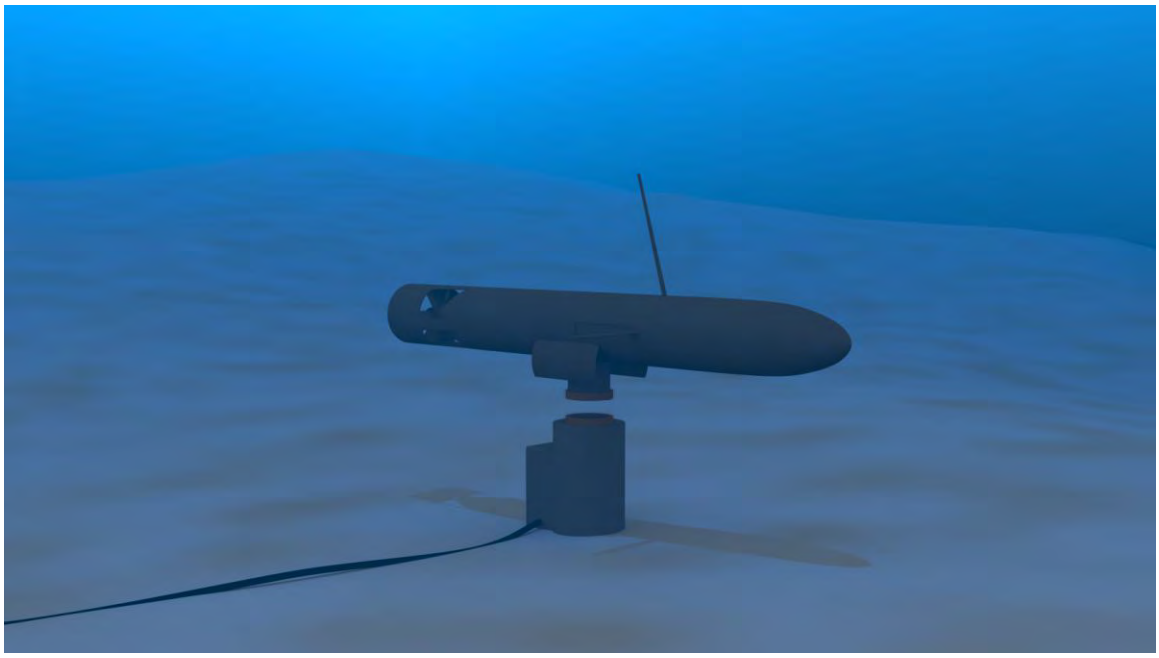

Figure 2. Nominal IPT docking system designed for charging different hull diameter AUVs (from [6]).

B. OBJECTIVE

The objective of this thesis research is to analytically and quantitatively determine the power transfer efficiency of two circular magnetically coupled coils at various air gaps. Power transfer efficiency measurements of the series-series compensated system were performed with and without ferrite tiles. The measured efficiency results were then compared to the calculated efficiencies for further analysis. Finally, power transfer efficiency was measured when the receiving coil and ferrite tiles were placed inside an aluminum AUV hull. Simulation of the two coil system was also performed using Agilent's advance design system (ADS). This thesis work was conducted in collaboration with the Space and Naval Warfare Systems Center (SSC) Pacific. They provided the transmitting coil, receiving coil and the aluminum AUV hull. SSC Pacific also suggested the operating conditions for this research.

C. THESIS ORGANIZATION

This thesis is organized into six chapters. In Chapter I, the motivation for IPT and the benefits of using of IPT to charge AUVs as well as the thesis objective is discussed.

In Chapter II we discuss the theory behind IPT, the concept of mutually coupled coils, and different IPT compensation topologies are introduced. Also in Chapter II, the IPT system efficiency equation is derived as well as the ideal matching load resistance as a function of the coil's internal resistance, mutual inductance and frequency. Based on the equations derived in Chapter II, in Chapter III we discuss the calculated system efficiency as a function of distance between the coils. The calculated results are then compared to system efficiency results simulated using ADS. Once the maximum achievable power transfer system efficiencies are calculated, they are compared to the measured efficiencies and discussed in Chapter IV. Due to the poor efficiency results shown in Chapter IV, in Chapter V we discuss several methods to increase power transfer efficiency. Finally in Chapter VI, we discuss areas of future work, summarize the work performed and present conclusions based on the thesis research.

II. BACKGROUND

A. INDUCTIVE POWER TRANSFER

In 1899 Nikola Tesla attempted to transmit power without wires. His goal was to transmit 300 kW of power using a 150 kHz carrier wave [7]. Tesla's attempt in wireless transmission ended in failure because he did not understand the dependency between the carrier wave and the transmitting antenna [4], [8]. Despite Tesla's failure to transmit power wirelessly he introduced a new field of study in WPT. WPT over long distances can be conducted using electromagnetic waves, but over shorter ranges, less than a meter, IPT between two magnetically coupled coils is the preferred method of power transfer.

Michael Faraday and Joseph Henry independently came to the conclusion that a time-varying magnetic field can produce an electric field, but the credit is normally given to Michael Faraday. After numerous experiments, Faraday was able to derive what is now called Faraday's law (in integral form)

$$\oint_C \vec{E} \cdot \vec{dl} = -\int_S \frac{\partial \vec{B}}{\partial t} \cdot \vec{ds}, \tag{1}$$

where $\vec{E}$ is the electric field vector over the contour of a loop and $\vec{B}$ is the magnetic field vector over the surface area of a loop.

The magnetic flux Φ passing through a closed loop is defined as

$$\Phi = \int_S B \cdot ds \tag{2}$$

and Eq. (1) can be simplified to

$$\oint_C \vec{E} \cdot \vec{dl} = -\frac{d\Phi}{dt}. \tag{3}$$

Using Eq. (3), we see that the time-varying magnetic flux Φ in a closed loop produces an induced electric motive force (emf) V. Faraday's law as written in Eq. (3) is for one turn of a loop. For a coil with N turns, Eq. (3) can rewritten as

$$V = -N\frac{\partial \Phi}{\partial t}. \tag{4}$$

A physical representation of a time-varying magnetic flux in a closed loop is shown in Figure 3.

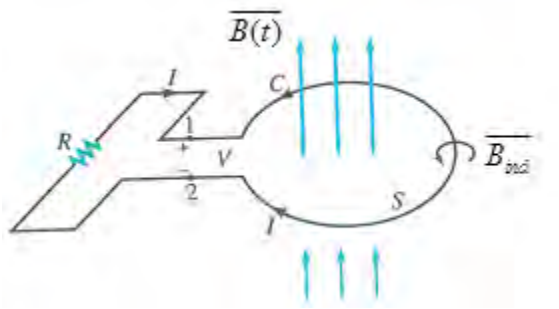

Figure 3. A closed loop in the presence of a changing magnetic flux (from [8]).

The direction of current flow shown in Figure 3 can be determined by Lenz's law. Lenz's law states the direction of current flow in the closed loop is always in a direction that opposes the change in magnetic flux $\Phi(t)$ that produced it [8]. Faraday was able to demonstrate that a time-varying magnetic field could induce an electric field, but could a time-varying current induce a magnetic field?

Andrè Ampère's was able to derive the relationship between a time-varying current and an induced magnetic field. Ampère was able to demonstrate the following law (in integral form)

$$\int_S (\nabla \times \vec{H}) \cdot \vec{ds} = \int_S \vec{J} \cdot \vec{ds} + \int_S \frac{\partial \vec{D}}{\partial t} \cdot \vec{ds}, \tag{5}$$

where $\vec{H}$ is the magnetic field intensity, $\vec{J}$ is the volume current density and $\vec{D}$ is the electric flux density. The surface integral of $\vec{J}$ is the equivalent to the conduction current and can be expressed as I_C [8]. Using Stokes theorem Eq. (5) can be rewritten as [8]

$$\oint_L \vec{H} \cdot \vec{dl} = I_C + \int_S \frac{\overrightarrow{\partial D}}{\partial t} \cdot \vec{ds}. \tag{6}$$

Maxwell also introduced the concept of displacement current,

$$I_d \triangleq \int_S J_d \cdot ds = \int_S \frac{\partial D}{\partial t} \cdot ds \tag{7}$$

where J_d is the displacement current density [8]. Now Eq. (6) can be rewritten as

$$\oint_C H \cdot dl = I_c + I_d = I, \tag{8}$$

where I is the total current in the loop. Through Maxwell's use of Ampère's law, Maxwell was able to show that a time-varying current can induce a magnetic field.

B. MUTUALLY COUPLED COILS

To demonstrate the concept of mutually coupled coils, we need to start with two coils situated near each other as shown in Figure 4.

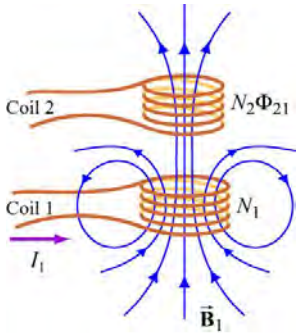

Figure 4. Alternating current in coil 1 is produces a time-varying magnetic flux in coil 2 (from [9]).

Coil 1 carries an alternating current defined as I_1. The current I_1 induces a magnetic flux in coil 2 denoted as Φ_{21}. Using Eq. (4), we can show that the induced emf in coil 2 due to the alternating current in coil 1 is

$$V_{21} = -N_2 \frac{\partial \Phi_{21}}{\partial t}. \tag{9}$$

Using the Biot-Savart law [9], we can show that the time-varying magnetic flux in coil 2 is proportional to the time-varying current in coil 1, and Eq. (9) can be expressed as

$$V_{21} = N_2 \frac{\partial \Phi_{21}}{dt} = M_{21} \frac{\partial I_1}{dt}, \tag{10}$$

where M_{21} is a proportionality constant of mutual inductance of coil 2 due to coil 1 and has units of henrys (H).

Using a similar approach as discussed earlier in Section II.B, we can derive the mutual inductance of coil 1 due to the alternating current in coil 2, as shown in Figure 5.

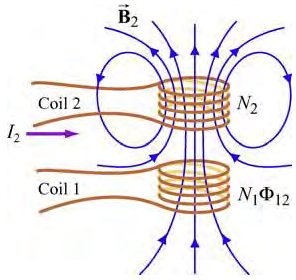

Figure 5. Alternating current in coil 2 is produces a time-varying magnetic flux in coil 1 (from [9]).

We start with coil 2 carrying an alternating current I_2. Due to I_2, a magnetic flux is induced in coil 1 Φ_{12}. The induced emf in coil 1 due to the time-varying current in coil 2 can be expressed as

$$V_{12} = -N_1 \frac{\partial \Phi_{12}}{\partial t}. \tag{11}$$

Using the Biot-Savart law, we see that the time-varying magnetic flux in coil 1 is proportional to the time-varying current in coil 2 and can be expressed as

$$V_{12} = N_1 \frac{\partial \Phi_{12}}{dt} = M_{12} \frac{\partial I_1}{\partial t}, \tag{12}$$

where the proportionality constant M_{12} is the mutual inductance of coil 1 due to coil 2. Using the reciprocity theorem, which combines Ampère's law and the Biot-Savat law, we can show that $M_{12} = M_{21}$ and both can now be expressed simply as M [9].

C. IPT TOPOLOGIES

An IPT system can be categorized as a closely coupled system or a loosely coupled system [10]. A closely coupled IPT system is a system where the magnetic coupling between coil 1 and coil 2, which are now referred to as the transmitting and receiving coils, respectively, is classified as good. Good is defined as a closely coupled system that has leakage inductances that are small compared to the magnetizing inductance between the two coils [10]. Closely coupled IPT systems typically have a magnetic core to guide the magnetic flux. An example of a closely coupled IPT system is a power transformer. A loosely coupled IPT system is characterized as a system where the magnetizing inductance between the transmitting and receiving coils is poor [10]. These systems typically do not have a magnetic core, and the magnetic inductance occurs over an air gap, causing the leakage inductance to be much greater than the magnetizing inductance. Some uses of loosely coupled IPT are wireless battery charging of cars and buses [4], [10]–[12], wireless battery charging of commercial products [4], and charging AUVs underwater [13], [14]. We use a loosely coupled IPT system for this research work.

Due to the poor coupling between the transmitting coil and the receiving coil, the power transfer efficiency can be poor. In order to improve efficiency in the loosely coupled IPT system, the transmitting and receiving coils must operate in resonance with each other, [10], [15]–[17]. An example of a loosely coupled IPT circuit model using series-series compensation is shown in Figure 6.

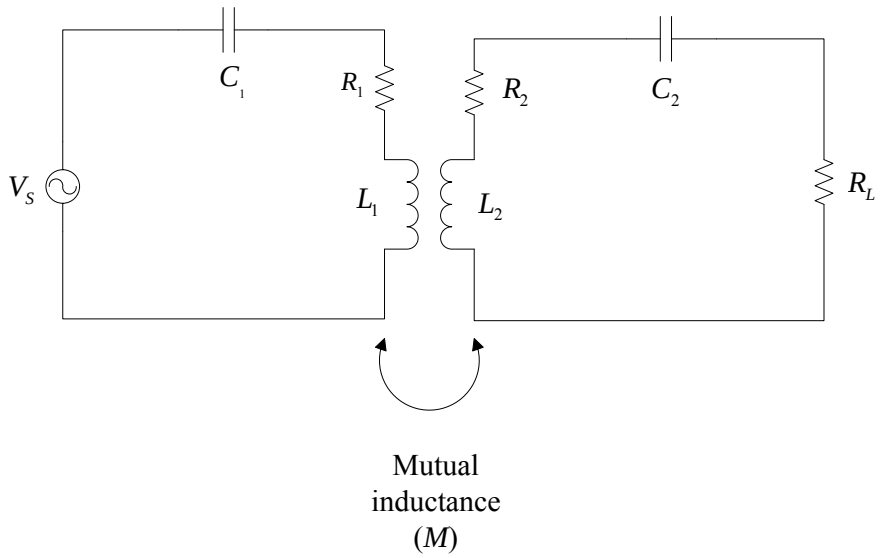

Figure 6. Simplified circuit model for a series-series compensated topology for a loosely coupled IPT system.

Resonance operation occurs when we impedance match the transmitting and receiving coils at the frequency of operation. At resonance the maximum power transfer efficiency of the system can be reached [17], [18]. To operate at resonance a compensating capacitor is chosen based on the inductance of the transmitting coil. The value of the capacitor is determined by using

$$C_1 = \frac{1}{L_1 \omega_0^2}, \tag{13}$$

where C_1 is the compensating capacitor for the transmitting coil, L_1 is the inductance of the transmitting coil and ω_0 is the angular frequency at which the IPT system will operate.

The value of the receiving coil's compensating capacitance can be determined using

$$C_2 = \frac{1}{L_2 \omega_0^2}, \tag{14}$$

where C_2 is the compensating capacitor for the receiving coil and L_2 is the inductance of the transmitting coil.

Most loosely coupled IPT systems follow a basic design similar to the one shown in Figure 7. The ac power source shown in Figure 7 should be operated at the coil's rated current and be allowed to have its voltage vary with the load [10] in order to control the current in the primary winding. Since the magnetic coupling is poor, operating the IPT system at rated current allows for the maximum possible coupling between the coils [10]. The transmitting and receiving coils' compensation, shown in Figure 7, can be determined using Eq. (13) and Eq. (14), respectively. The transmitting and receiving coils should be made to maximize power transfer efficiency as discussed in Chapter V. For maximum power transfer to the load shown in Figure 7, the load should be matched for ω_0, M, and the system resistances, as will be shown in Section II.D.2.

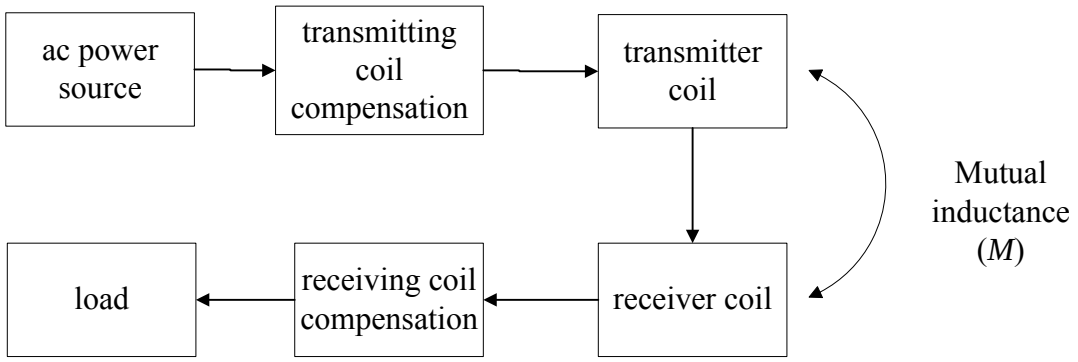

Figure 7. Basic loosely coupled IPT design block diagram.

There are four basic transmitting and receiving coil compensation topologies: series-series compensation, as shown in Figure 6; series-parallel, as shown in Figure 8; parallel-series compensation, as shown in Figure 9 and parallel-parallel compensation, as shown in Figure 10. The placement of the compensating capacitance determines the compensation topology. For example, a series-parallel topology indicates that C_1 is in series with the transmitting coil and C_2 is in parallel with the receiving coil, as shown in Figure 8.

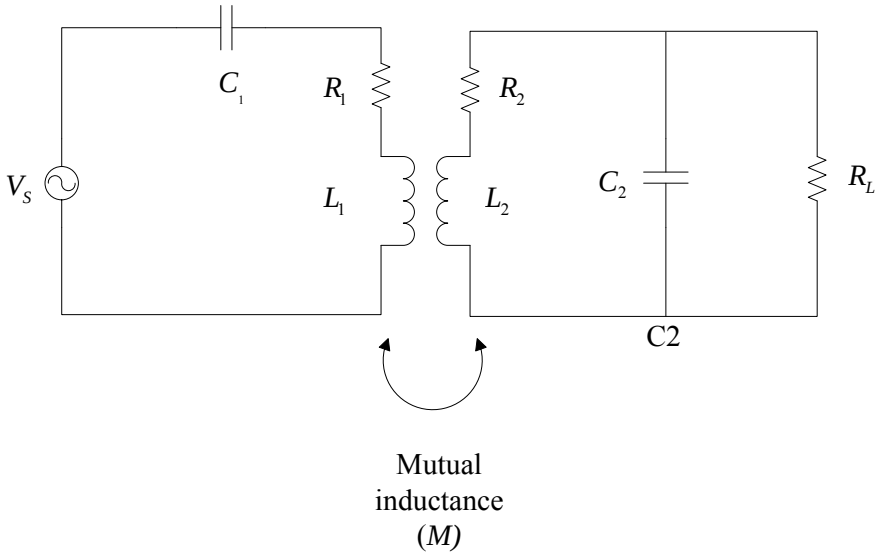

Figure 8. Simplified circuit model for a series-parallel compensation topology for an IPT system.

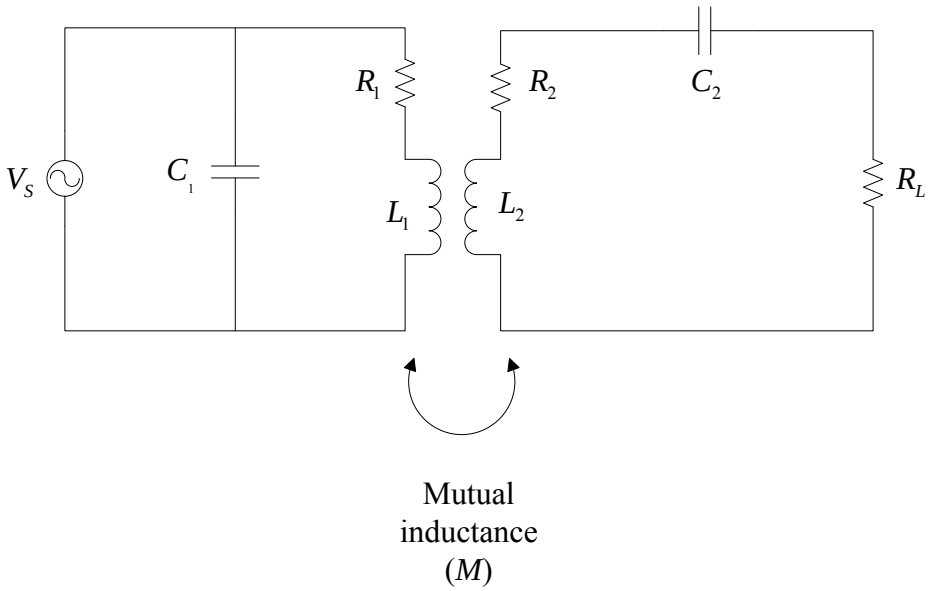

Figure 9. Simplified circuit model for a parallel-series compensation topology for an IPT system.

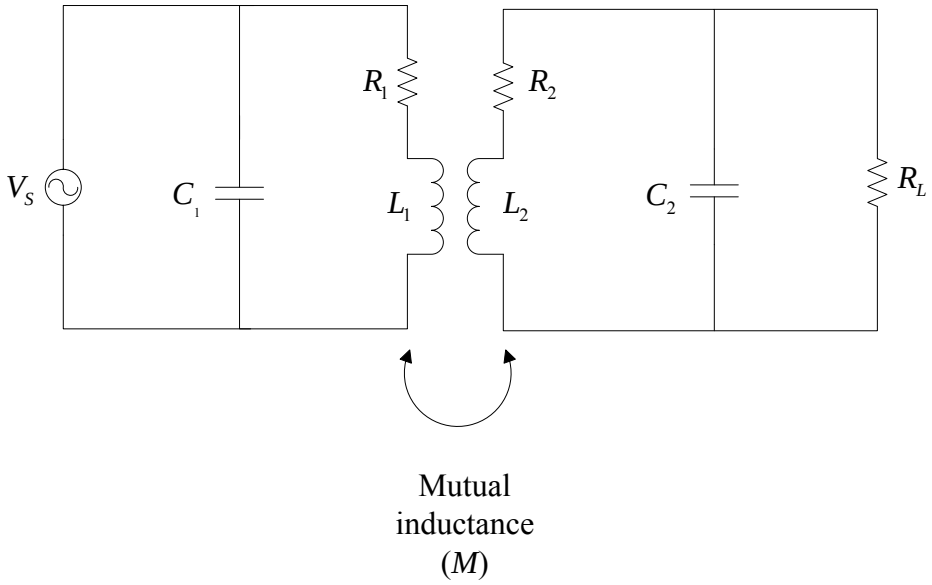

Figure 10. Simplified circuit model for a parallel-parallel compensation topology for an IPT system.

The selection of a compensation scheme depends on the use of the IPT system. For applications involving long tracks, such as battery charging for a train or buses, series compensation for the transmitting coil is recommended [10]. In applications where the ac power source voltage needs to be reduced, parallel compensation for the transmitting coils is recommended [10]. For the receiving coil, series compensation is recommended if the load is going to be a dc bus and parallel compensation is recommended if the coil is going to be used for battery charging [10]. The selected compensation method used in this thesis is series-series compensation. The main consideration in the selection of this topology is that series-series compensation matches the topology used by SSC Pacific [3].

D. EFFICIENCY AND IDEAL LOAD RESISTANCE

1. System Efficiency

Using the circuit model for series-series compensation, we can determine the overall system efficiency η by deriving equations for power delivered by the transmitting coil P_t and power delivered to the load P_L. When the IPT system is operating at ω_0,

Kirchhoff's voltage law (KVL) equations for the system can be expressed in phasor form as ($e^{+j\omega t}$ time convention assumed and suppressed):

$$V_S = \left(R_1 + j\omega_0 L_1 + \frac{1}{j\omega_0 C_1} \right) I_1 + j\omega_0 M I_2 \tag{15}$$

for the transmitter side of the circuit, and

$$0 = \left(R_2 + j\omega_0 L_2 + \frac{1}{j\omega_0 C_2} + R_L \right) I_2 + j\omega_0 M I_1 \tag{16}$$

for the receiver side of the circuit. The parameters for Eq. (15) and (16) are:

V_s: Voltage supply;
R_1: Internal resistance of the transmitting coil;
R_2: Internal resistance of the receiving coil;
L_1: Inductance of transmitting coil;
L_2: Inductance of the receiving coil;
C_1: Compensating capacitance for the transmitting coil;
C_2: Compensating capacitance for the receiving coil;
I_1: Transmitting coil current;
I_2: Receiving coil current;
M: Mutual inductance between the transmitting and receiving coils.

The next steps are to determine the transmitter side impedance Z_1, the receiver side impedance Z_2, the mutual impedance of the two coupled coils Z_m and the load impedance Z_L, which can be expressed, respectively, as

$$Z_1 = R_1 + j\omega_0 L_1 + \frac{1}{j\omega_0 C_1}, \tag{17}$$

$$Z_2 = R_2 + j\omega_0 L_2 + \frac{1}{j\omega_0 C_2}, \tag{18}$$

$$Z_m = j\omega_0 M, \tag{19}$$

and

$$Z_L = R_L. \tag{20}$$

Substituting Eqs. (17) through (20) into Eq. (15) and Eq. (16), we can express the series-series IPT system in terms of system impedances

$$V_S = Z_1 I_1 + Z_m I_2, \tag{21}$$

$$0 = (Z_2 + Z_L) I_2 + Z_m I_1. \tag{22}$$

Solving Eq. (21) for I_1, we can determine the transmitting coil current

$$I_1 = \frac{V_S - Z_m I_2}{Z_1}. \tag{23}$$

Performing a similar process with Eq. (22), we get

$$I_2 = \frac{-Z_m I_1}{(Z_2 + Z_L)}. \tag{24}$$

Substituting Eq. (24) into Eq. (23), we can express I_1 in terms of only the ac voltage source and system impedances:

$$I_1 = \frac{V_S (Z_2 + Z_L)}{Z_1 Z_2 - Z_m}. \tag{25}$$

We can also express I_2 in terms of the ac voltage source and system impedances by substituting Eq. (23) into Eq. (24) to get

$$I_2 = \frac{-V_S Z_m}{Z_1 (Z_2 + Z_L) - Z_m^2}. \tag{26}$$

A useful parameter to derive next is the reflected impedance Z_r. The reflected impedance is the equivalent impedance of the receiving coil, receiver capacitance, and the load impedance reflected onto the transmitting side. In order to get to an expression of reflected impedance, we need to determine the dependent voltage of the transmitting coil due the receiving coil V_{12}

$$V_{12} = -Z_m I_2. \tag{27}$$

Substituting Eq. (24) into Eq. (27) gives an expression of the transmitter dependent voltage in terms of I_1:

$$V_{12} = \frac{Z_m^2}{(Z_2 + Z_L)} I_1. \tag{28}$$

By dividing Eq. (28) by Eq. (25), we obtain an expression for the reflected impedance as

$$Z_r = \frac{V_{12}}{I_1} = \frac{Z_m^2}{(Z_2 + Z_L)}. \tag{29}$$

With the expression for the reflected impedance derived, we can determine the input impedance Z_{in}. The input impedance of the series-series IPT is the series addition of the reflected impedance Eq. (29) and transmitter side impedance Eq. (17)

$$Z_{in} = Z_1 + \frac{Z_m^2}{(Z_2 + Z_L)}. \tag{30}$$

Now that all the system impedance equations are derived, we derive P_t by substituting Eq. (30) into the definition of dissipated power

$$P_t = \frac{1}{2}\mathrm{Re}(Z_{in}^*)\left|I_1\right|^2. \tag{31}$$

We substitute the input impedance Eq. (30) into Eq. (31) to obtain an expression for P_t in terms of system impedances and the ac source voltage:

$$P_t = \frac{1}{2}\frac{\mathrm{Re}(Z_{in}^*)(Z_2 + Z_L)^2}{[Z_1 + (Z_2 + Z_L) - Z_m^2]^2} V_S^2. \tag{32}$$

From the definition of dissipated power, P_L of the system can be expressed as

$$P_L = \frac{1}{2}\mathrm{Re}(Z_L^*)\left|I_2\right|^2. \tag{33}$$

Substituting Eq. (26) into Eq. (33), we get expression for P_L in terms of system impedances and the ac source voltage as

$$P_L = \frac{1}{2}\frac{\mathrm{Re}(Z_L^*)Z_m^2}{[Z_1(Z_2+Z_L)-Z_m^2]^2}V_S^2. \tag{34}$$

We divide Eq. (34) by Eq. (33) to obtain η in terms of system impedances:

$$\eta = \frac{P_L}{P_t} = \frac{\mathrm{Re}(Z_L^*)Z_m^2}{\mathrm{Re}(Z_{in}^*)(Z_2+Z_L)^2}. \tag{35}$$

As discussed previously, when the transmitting and receiving coils are properly compensated and operating at a resonant frequency, a strong magnetic coupling between the transmitting and receiving coils exists. This leads to the most efficient power transfer because no reactive power is transferred between the coils and Eq. (35) can now be expressed in terms of ω_0, resistances and M as

$$\eta = \frac{R_L(\omega_0 M)^2}{R_1(R_2+R_L)^2+(\omega_0 M)^2(R_2+R_L)}. \tag{36}$$

System efficiency can also be expressed in terms of the magnetic coupling coefficient k and quality factor Q. It was shown that the maximum achievable transfer efficiency is dependent on the coils composition and can be given as [19]

$$\eta_{\max} = \frac{(kQ)^2}{(1+\sqrt{1+(kQ)^2})^2}, \tag{37}$$

where Q is the combined quality factor of both coils and k is a unitless value between 0 and 1.

The magnetic coupling coefficient expresses how well the transmitting and receiving coils are magnetically coupled together. The higher the value of k, the better the magnetic coupling is between the two coils. The magnetic coupling coefficient is defined as [18]

$$k \equiv \frac{M}{\sqrt{L_1 L_2}}. \tag{38}$$

Quality factor is a measure of how well a single coil is operating. An overall combined system quality factor is defined as [19]

$$Q \equiv \sqrt{Q_1 Q_2}, \tag{39}$$

where Q_1 is the quality factor of the transmitting coil and Q_2 is the quality factor of the receiving coil. The individual quality factors are defined as [19], [20]

$$Q_{1,2} \approx \frac{\omega_0 L_{1,2}}{R_{ac1,2}}, \tag{40}$$

where ω_0 is the operating angular frequency, $L_{1,2}$ is the inductance of either the transmitting or receiving coil and $R_{ac1,2}$ is the ac resistance of the coil at the frequency of operation.

2. Ideal Load Resistance for an IPT System

Based on Eq. (36), we can show that there is an ideal matched load resistance for a given air gap. To determine the ideal matched load resistance, we need to differentiate Eq. (36) with respect to R_L, set the result equal to zero, and solve for R_L. The resulting $R_{L,matched}$ can be expressed as [20]

$$R_{L,matched} = \sqrt{R_2^2 + (\omega M)^2 \frac{R_2}{R_1}}. \tag{41}$$

The full derivation for $R_{L,matched}$ can be found in Appendix A. As the distance between the transmitting and receiving coils increases, magnetic flux between the coils decreases, as discussed in Section III.A. This decrease in magnetic flux decreases *M* between the coils. With all other parameters held constant, the decrease of *M* causes a decrease in $R_{L,matched}$.

E. SUMMARY

In this chapter we discussed the fundamental principles of magnetic induction. Using Faraday's laws, we showed that a time-varying magnetic field can induce a time-varying current and a time-varying current can induce a time-varying magnetic field. Next, we discussed the various IPT topologies and the need for compensating capacitors to achieve maximum power transfer efficiency. Finally, based on the series-series

compensated IPT system, equations for power transfer efficiency and matched load resistance were derived.

In the next chapter we calculate the required compensating capacitance, the mutual inductance and the power transfer efficiency of a series-series compensated system. The numerically calculated results are then compared to the power transfer efficiency simulation results from ADS.

THIS PAGE INTENTIONALLY LEFT BLANK

III. CALCULATION OF SYSTEM EFFICIENCY FOR COILS IN AIR

A. COMPENSATING CAPCITANCE AND MEASUREMENT OF COIL VALUES

SSC Pacific provided two coils for use in this research. Both coils consist of 18 gauge wire (AWG) tightly wound in a circular geometry, as shown in Figure 11. The coils were potted with a clear urethane material to protect the 18 gauge wire from seawater corrosion. The urethane material has a magnetic permeability of 1.0. A thermal epoxy was also applied to each coil to assist with thermal dissipation when the coils were in operation [3]. Each coil consists of 20 turns and has a radius of 60.325 mm as measured from the last turn, as shown in Figure 11. The coil has a total outer radius of 63.5 mm as measured from the outer diameter of the urethane potting material.

Figure 11. Urethane potted coil placed next to its wooden mounting stand.

SSC Pacific determined the desired frequency of operation for the coils to be 100 kHz. It was shown in [3] that at operating frequencies at or below 100 kHz, there was little difference in resistance and reactance values when the measurements were taken in air or in seawater. At frequencies above 100 kHz, the resistance of seawater begins to increase the equivalent internal resistance of the coils. The increase in internal resistance causes a decrease in efficiency and should be avoided.

The inductance of the transmitting and receiving coils was measured with an Array Solutions Ultra High Frequency (UHF) Vector Network Analyzer (VNA) at 100 kHz. From the measurements, the transmitting coil has an internal resistance of $R_1 = 1.322\ \Omega$ and an inductance of $L_1 = 83.3454\ \mu$H, as shown in Figure 12.

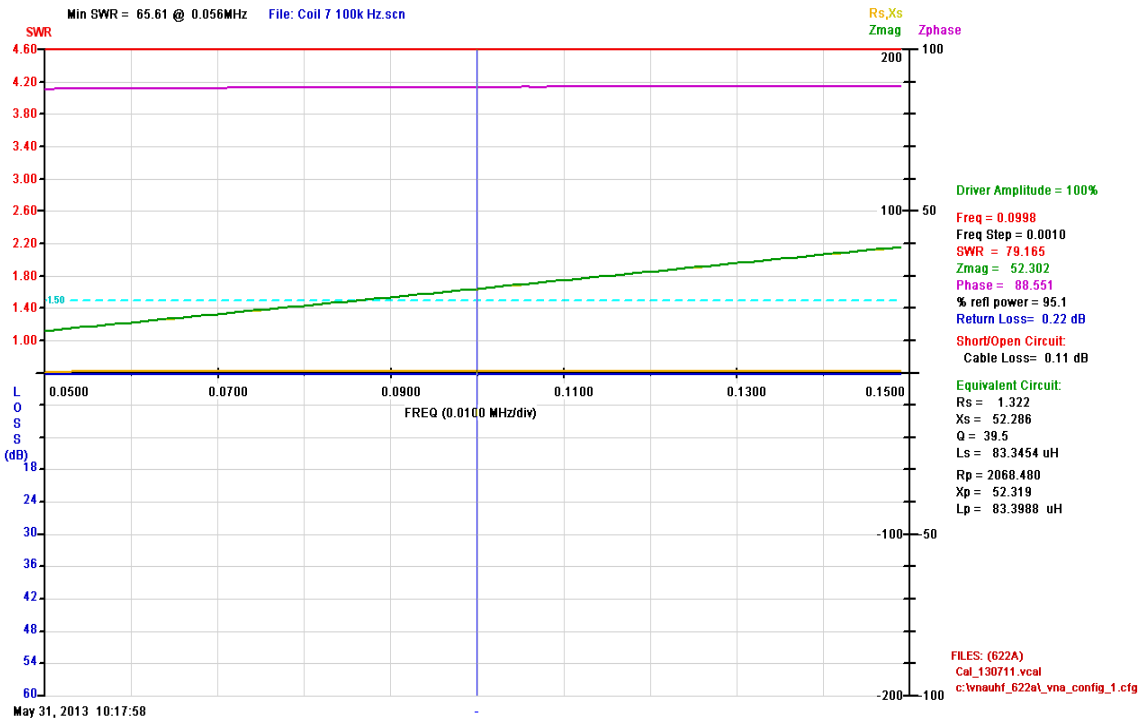

Figure 12. Plot of the transmitting coil's measured impedance versus frequency.

Using Eq. (13) and the measured inductance of the transmitting coil, we calculated the compensating capacitance for the coil to be 30.39 pF. Connecting the VNA in series with an IET labs capacitance substituter box and the coil, we then

measured the capacitance and coil combination. It was determined that an actual capacitance (as read on the capacitance substituter box) of 29.8 pF worked the best to compensate for the coil's inductance. We determined the proper compensating capacitance by adjusting the capacitance substituter box until the phase angle, the purple line in Figure 13, was close to zero at 100 kHz.

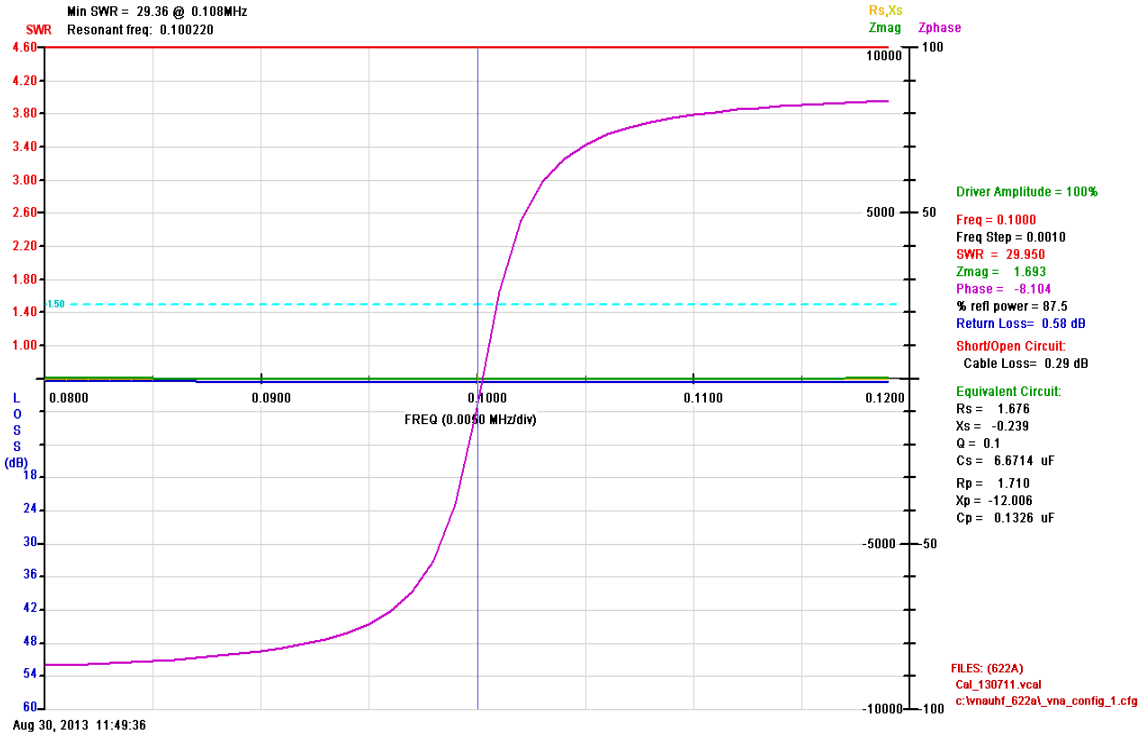

Figure 13. Plot of the transmitting coil's impedance when connected with the compensating capacitance of 29.8 pF versus frequency.

Following the same methodology as for the transmitting coil, the receiving coil's internal resistance and inductance was measured as $R_2 = 1.440\ \Omega$ and $L_2 = 83.0183\ \mu H$, respectively, as shown in Figure 14.

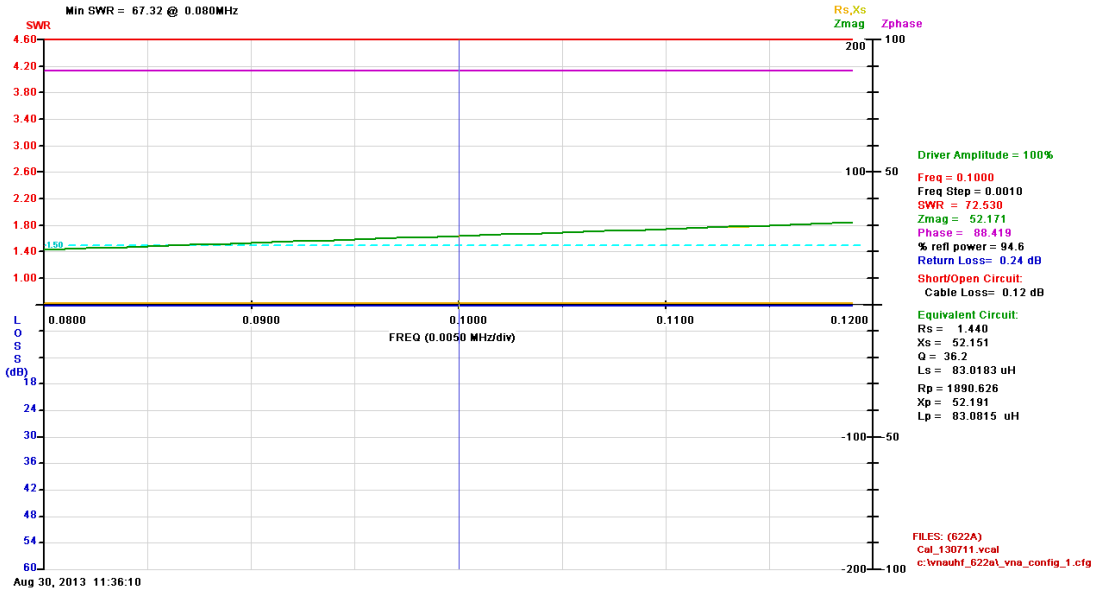

Figure 14. Plot of the receiving coil's measured impedance versus frequency.

From Eq. (14) the coupling capacitance of the receiving coil was calculated as 30.50 pF, but the actual value used was 29.5 pF because it worked best to compensate for the coil's inductance, as shown in Figure 15. Using 29.5 pF, we achieved close to zero phase angle at 100 kHz. The coil values are summarized in Table 1.

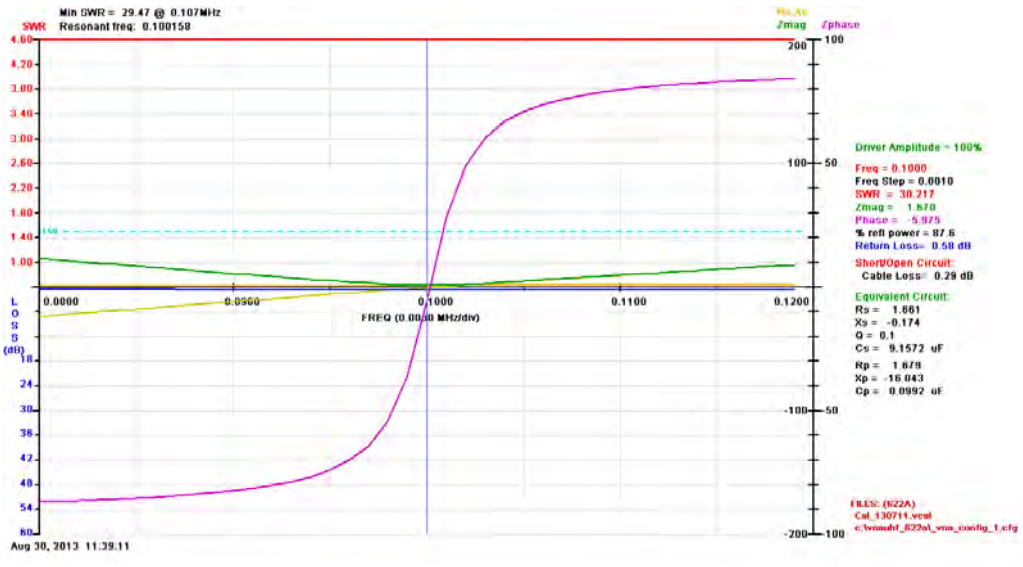

Figure 15. Plot of the receiving coil's measured impedance when connected with a compensating capacitor of 29.5 pF versus frequency.

Table 1. Summary of transmitting and receiving coil values at 100 kHz.

Operating frequency is 100 kHz	Transmitting coil	Receiving coil	units
Coil internal resistance	1.322	1.44	ohms
Coil inductance	83.3545	83.3271	microhenrys
Actual coupling capacitance	29.5	29.5	picofarads
Coil turns	20	20	turns
Coil radius	60.325	60.325	milimeters

B. CALCULATATION OF *M*, $R_{L,matched}$, AND η

In order to calculate power transfer efficiency, we need to first determine the mutual inductance between the coils. The mutual inductance between two coils varies depending on the size and shape of the coils. The exact-closed form equation for mutual inductance of two circular coils in air can be expressed as [3]

$$
\begin{aligned}
M &= 2\mu_0 \frac{\sqrt{A+B}}{B}[(1-\frac{\beta^2}{2})K(\beta)-E(\beta)] \\
A &= \frac{a^2+b^2+D^2}{a^2b^2} \\
B &= \frac{2}{ab} \\
\beta &= \sqrt{\frac{2b}{a+b}}
\end{aligned}
\tag{42}
$$

where a is the radius of the transmitting coil; b is the radius of the receiving coil; D is the distance between the transmitter coils; μ_0 is the magnetic permeability of air equal to $4\pi(10^{-7})$; $K(\beta)$ is a first order elliptic integral and $E(\beta)$ is a second order elliptic integral.

To calculate M, $R_{L,matched}$, and η, a Matlab script file was written using Eqs. (36), (41) and (42). The Matlab script file can be found in Appendix B. Mutual inductance, matched load resistance and power transfer efficiency were determined as a function of distance between the two coils. A summary of the results is shown in Table 2.

Table 2. Computed mutual inductance, matched load resistance and power transfer efficiency as a function of the distance between the transmitting and receiving coils.

D (mm)	M (uH)	RL, matched (ohms)	power transfer efficiency (%)
16	43.49	27.15	90.7
20	37.31	23.3	89.3
25	31.35	19.59	87.4
30	26.70	16.7	85.4
35	23.00	14.39	83.2
40	19.91	12.49	81
45	17.37	10.91	78.4
50	15.23	9.59	75.8
55	13.41	8.47	73
60	11.86	7.51	70.1
65	10.52	6.69	67.1
70	9.37	5.99	63.9
75	8.37	5.38	60.6
80	7.50	4.86	57.3
85	6.74	4.4	53.9
90	6.07	4.01	50.4
95	5.48	3.66	47
100	4.96	3.36	43.6
105	4.50	3.1	40.3
110	4.09	2.87	37
120	3.40	2.5	30.9
130	2.86	2.22	25.4
140	2.41	2	20.5
150	2.06	1.84	16.5

Using the data in Table 2 and plotting *M* versus *D,* we notice that as *D* increases, *M* decreases, as shown in Figure 16. The reason for this decreasing mutual inductance is due to decreasing magnetic flux linking the two coils.

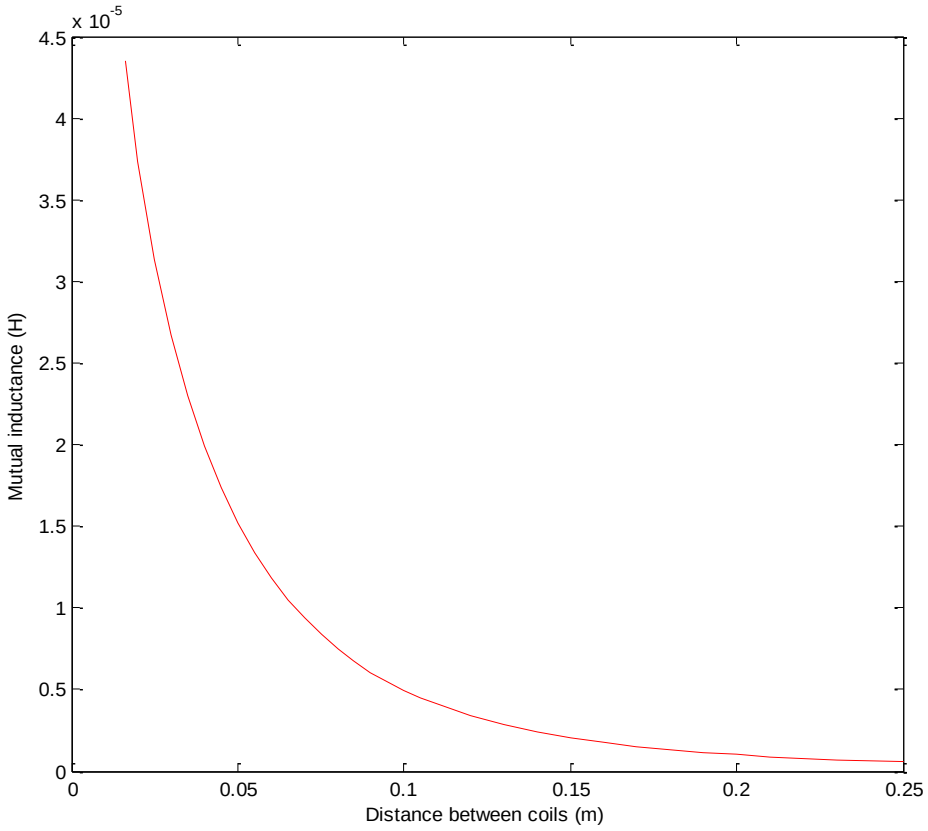

Figure 16. Graph of mutual inductance versus the distance between the receiving coil and transmitting coil.

Mutual inductance has a direct correlation to power transfer efficiency as shown in Eq. (36). A plot of system efficiency versus mutual inductance is shown in Figure 17. As mutual inductance decreases, the power transfer efficiency of the IPT system decreases. System efficiency decreases because as the distance between the coils increases, the amount of magnetic flux linkage between the coils decreases. This causes less power transfer and lower efficiency. From Figure 17, we can conclude that for maximum power transfer to occur we need to minimize the distance between the coils.

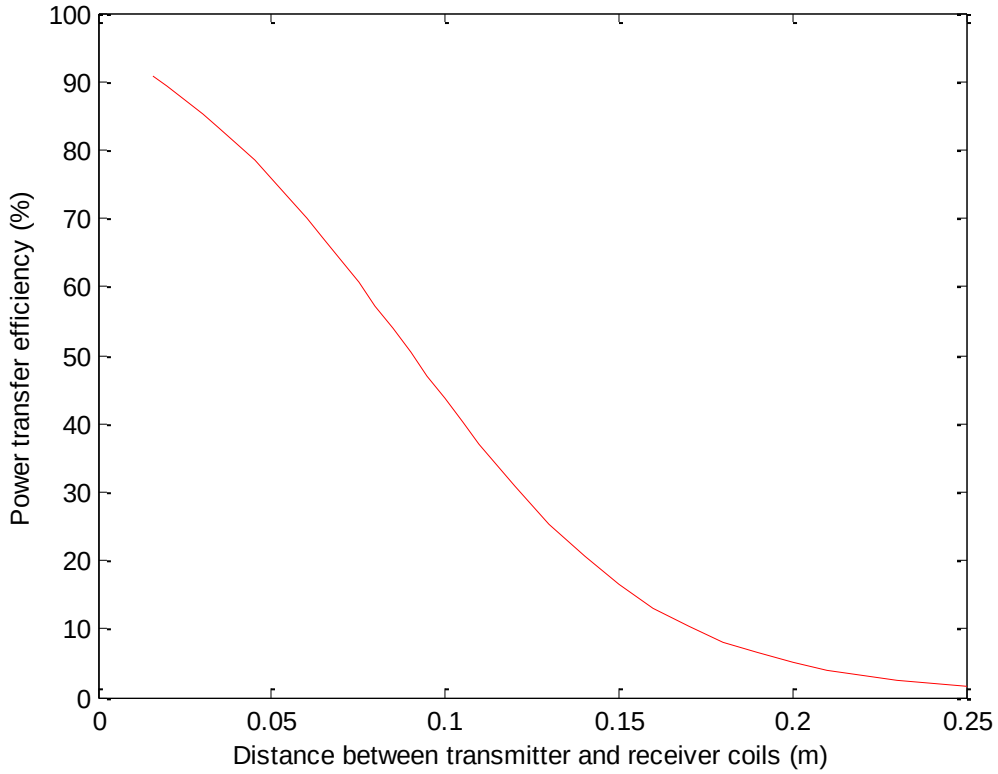

Figure 17. Power transfer efficiency as a function of the distance between coils.

C. POWER TRANSFER EFFICIENCY WITH ADS

The results of Eqs. (36) and (42) were compared to those given by an ADS simulation model of a series-series compensated circuit. The operating frequency of the model was varied from 50 kHz to 100 kHz and mutual inductance was varied from 43.4 μH to 0.559 μH. The load resistance of the IPT was fixed at 27.16 Ω, which corresponds to a $R_{L,matched}$ when the coils were 16 mm apart. The ADS simulation model with these values is shown in Figure 18, and the plotted results are shown in Figure 19. As shown in Figure 19, marker 1, the ADS simulation determined power transfer efficiency to be 90.4 percent. The difference between the calculated and ADS values for power transfer efficiency was 0.3 percent, which can be considered negligible. The ADS model was redone using $R_{L,matched}$ for various air gaps, and the efficiencies were

compared to the values in Table 2. The differences between ADS and the calculated values were small and could be ignored. These results verified that the equations derived in Chapters II and III are valid.

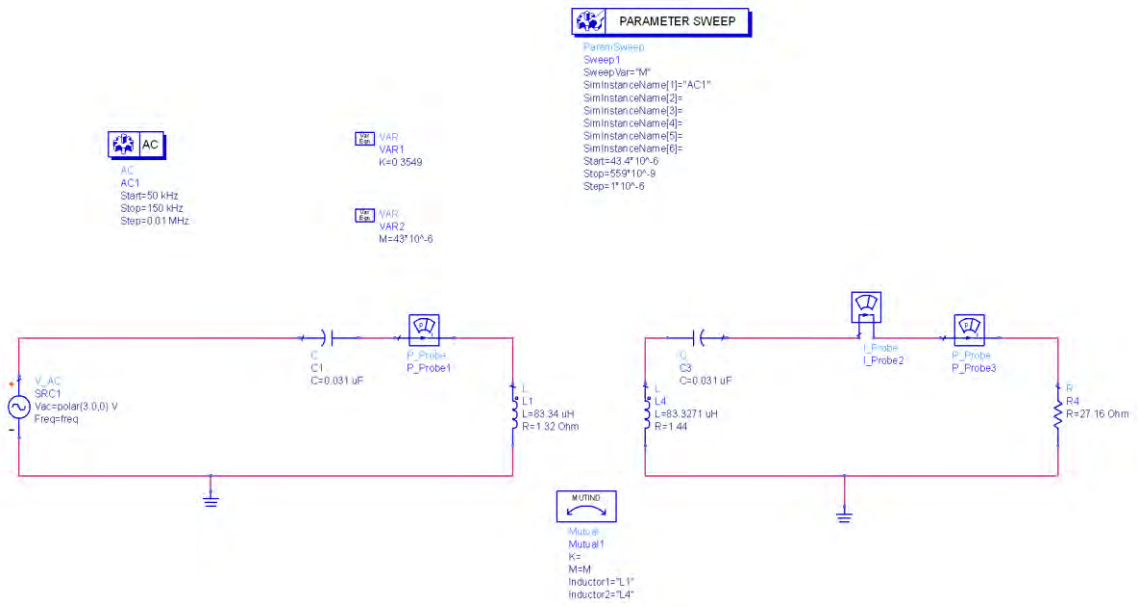

Figure 18. ADS simulation model of a series-series compensated IPT topology with a matched load resistance at 16 mm.

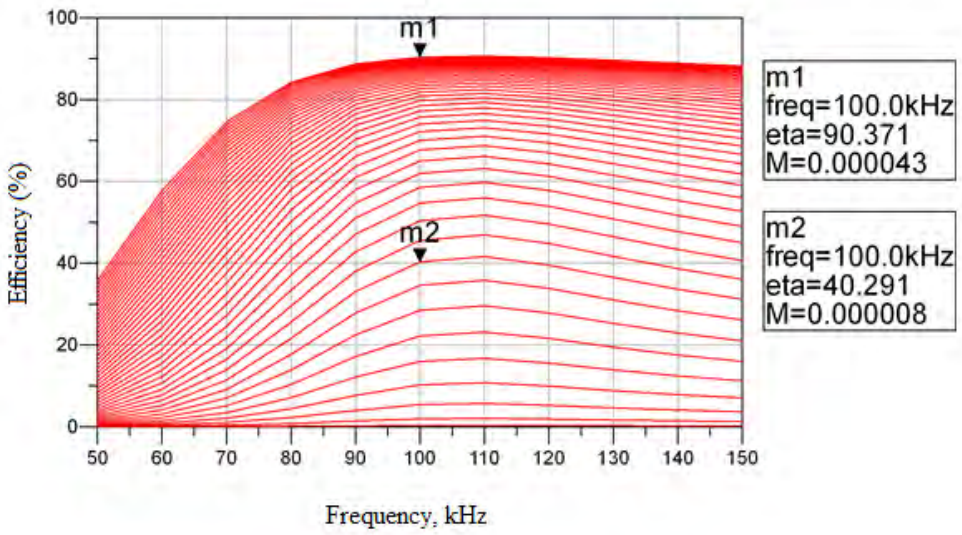

Figure 19. ADS simulation results of power transfer efficiency when load resistance is matched for a 16 mm air gap.

D. THE EFFECT OF A MATCHED LOAD RESISTANCE ON POWER TRANSFER EFFICIENCY

The load resistance of the IPT system has an important function in power transfer efficiency. Marker 2, as shown in Figure 19, was placed on a mutual inductance line equivalent to an air gap of 75 mm. The calculated power transfer efficiency with an air gap of 75 mm was 60.6 percent. The ADS simulated efficiency was 40.3 percent, a difference of 20.3 percent. The difference was attributed to not using the matched load resistance associated with an air gap of 75 mm.

For maximum power transfer efficiency to occur, the load must be matched to the air gap. For an IPT system with an air gap of 75 mm, the matching load resistance should be $5.38\,\Omega$, as shown in Table 2. The ADS simulation was redone using the 75 mm matched load resistance. The result of the ADS simulation is shown in Figure 20. At an air gap of 75 mm, the system efficiency determined by ADS was 59.3 percent or 1.3 percent different from the calculated value; the difference between the calculated efficiency and the ADS simulation was within numerical accuracy and can be ignored. We also note the change in efficiency when the air gap was at 16 mm. The efficiency dropped from 91.1 percent to 78.0 percent when the load resistance changed from 27.16

Ω to 5.38 Ω. This demonstrates that lowering the resistance when the air gap is smaller does not help efficiency. As shown in Figure 19 and Figure 20, the selection of a matched load resistance is important to the IPT power transfer efficiency.

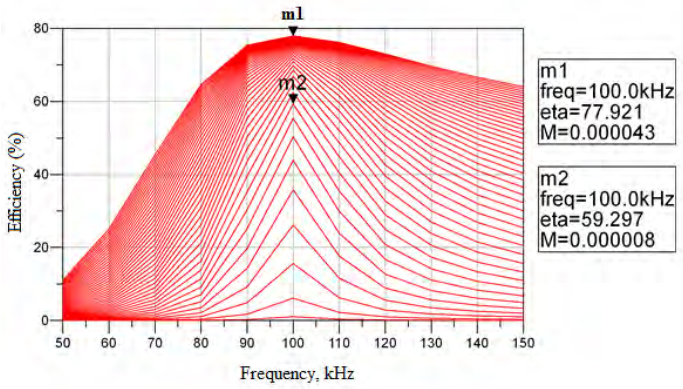

Figure 20. ADS graph of power transfer efficiency when load resistance is matched for a 75 mm air gap.

E. SUMMARY

It was shown that there is a negligible difference between the calculated values and those determined by the ADS simulation. We also saw the importance of having the proper matched load resistance for a given air gap and that decreasing the load resistance does not help efficiency when the air gap is small nor does increasing the load resistance help efficiency when the air gap is large.

THIS PAGE INTENTIONALLY LEFT BLANK

IV. MEASURED POWER TRANSFER EFFICIENCY

A. POWER TRANSFER EFFICIENCY

1. System Setup

The transmitting and receiving coils were connected following the circuit model shown in Figure 6. The power supply for the system was provided by an Agilent 33220A function generator connected in series with a Krohn-Hite 50 Watt amplifier. The capacitances were provided by two capacitance substituter boxes. Using a capacitance substituter box allowed for easier resonance matching of the coils. An IET labs resistance substituter was used for the load resistance. Using the resistance substituter box allowed for the ease of changing load resistance to correspond to a given air gap. The coils were attached to wooden stands using zip ties for support and ease of movement. The entire system setup is shown in Figure 21. The coil on the left in the photo is transmitting.

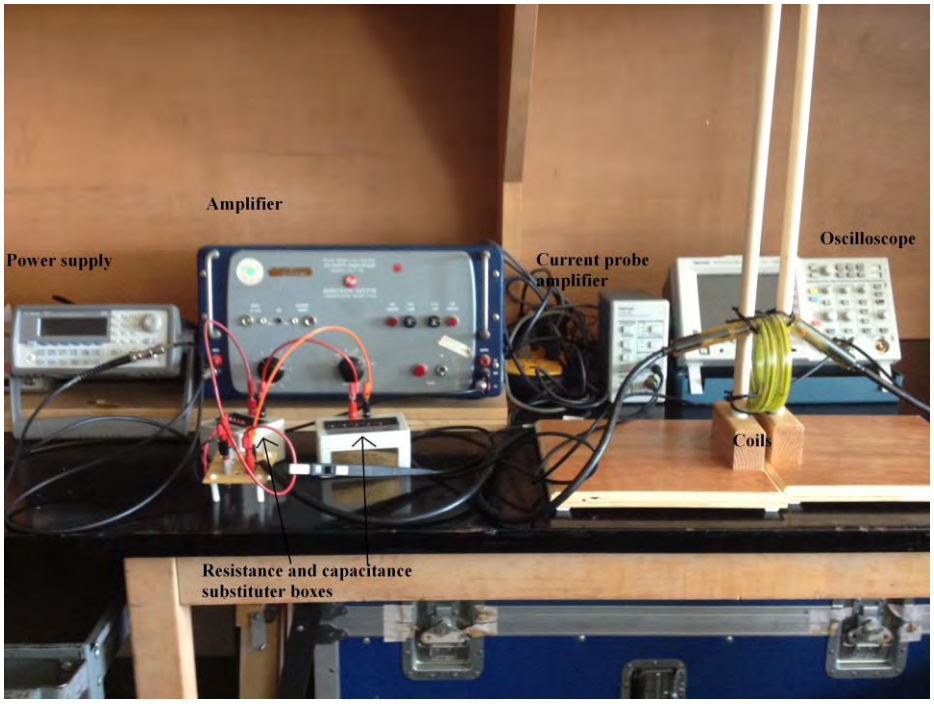

Figure 21. Photograph of the IPT system equipment.

2. Power Transfer Efficiency Measurement Procedure

Voltage measurements were taken across the transmitting coil using a Tektronix TDS 3032B oscilloscope. The current measurements were taken in series with the transmitting coil using a Tektronix TCPA 300 Amplifier and a TCP 305A current probe. The phase angle between the voltage and current waveforms was measured using the oscilloscope and converting the time between the voltage and current zero crossings to a corresponding phase angle. The load voltage and current were taken at the resistance substituter box using the oscilloscope and current probe. The distance between the coils was measured from the outer edge of the transmitting coil to the outer edge of the receiving coil, as shown in Figure 22. Due to the zip ties and the thickness of the urethane material, the closest distance between the coils attainable was 16 mm. The distance between the coils was varied from 16 mm to 150 mm.

At each distance increment, the load resistance was changed in accordance with Eq. (40). After the load resistance was changed the transmitted voltage, current and phase angle between the voltage and current was measured. The transmitted power was determined using

$$P_t = V_{rms} I_{rms} \cos\theta, \tag{43}$$

where P_t, V_{rms}, I_{rms}, and θ are the power, rms voltage, rms current, and phase angle, respectively, measured at the transmitting coil. The power delivered to the load was determined using

$$P_L = V_L I_L, \tag{44}$$

where P_L is the power delivered to the load, V_L and I_L are the load voltage and load current, respectively. Power transfer efficiency of the system was determined using Eq. (35).

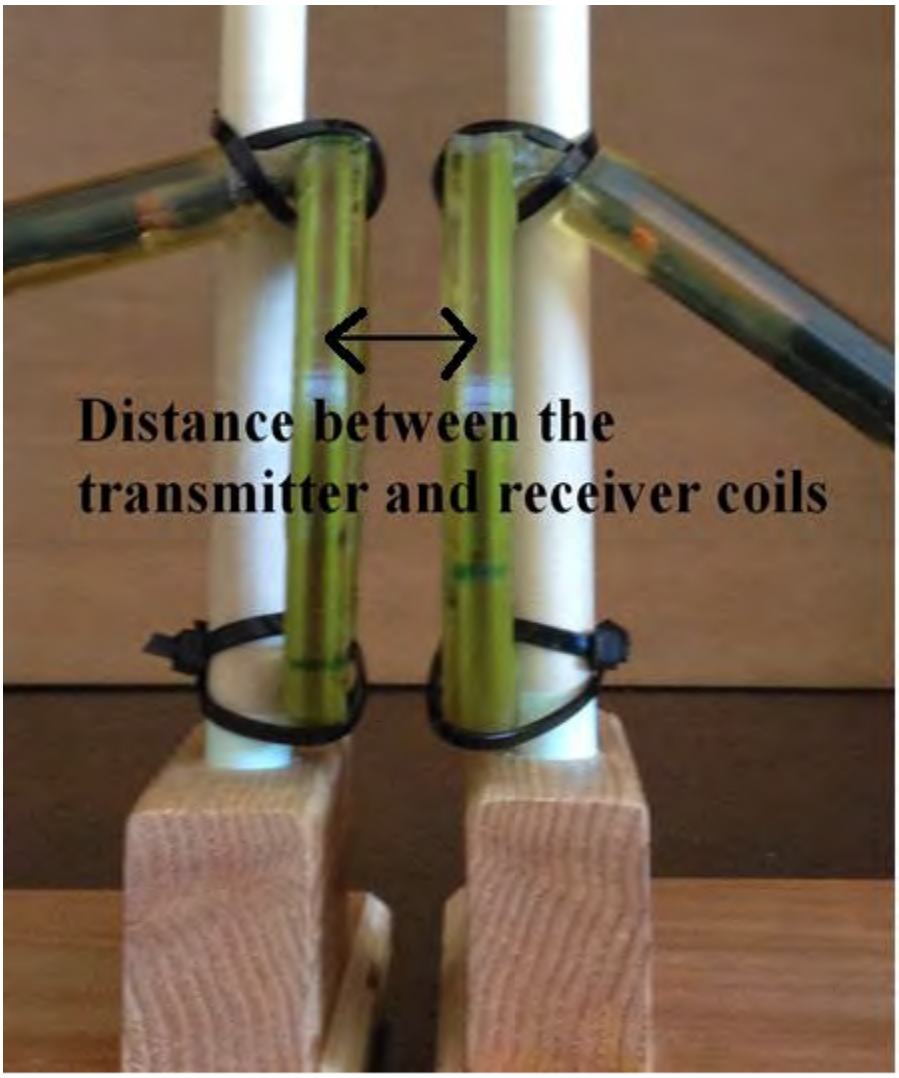

Figure 22. Photograph depicting how the distance between the coils was measured.

3. Measured Power Transfer Efficiency

Using the procedure discussed in Section IV.A.2, we moved the two coils apart, and the power transfer efficiency was measured and graphed, giving the results shown in Figure 23. At all distance increments, the measured power transfer efficiency never attained the values calculated in Table 2. The closest agreement between measured and calculated efficiencies was at the smallest air gaps (between 16 mm to 30 mm). At these distances the magnetic flux coupling between the coils was the strongest. At 16 mm the measured efficiency is within 3 percent of the calculated value, and at 30 mm the measured efficiency is within 8 percent of the calculated value. At distances greater than

30 mm the difference between measured and calculated efficiencies is greater than 10 percent. A complete set of measured data can be found in Appendix C.

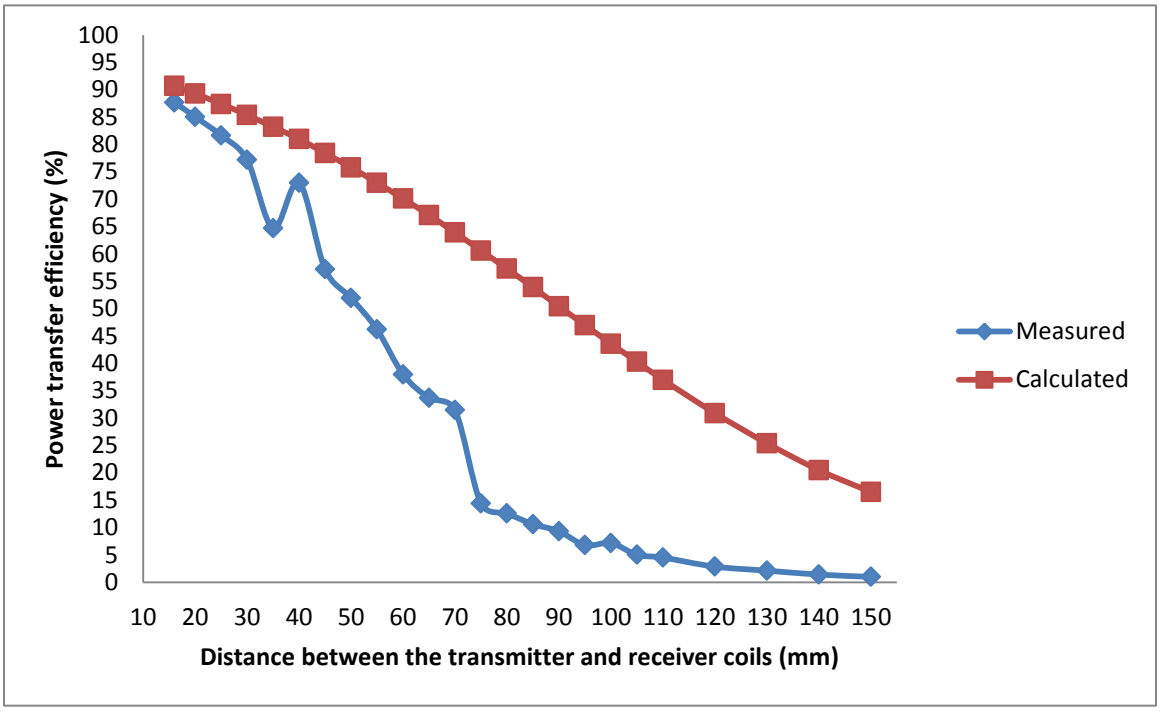

Figure 23. Graph of measured and calculated power transfer efficiency as a function of distance between the transmitting and receiving coils.

Efficiency increases from 64 percent at 35 mm to 73 percent at 40 mm, instead of decreasing as it should with an increasing air gap. The discrepancy can be due to how the phase angle was measured using the oscilloscope. Phase angle was determined by reading the time between the voltage and current zero crossings and converting this time to a phase angle. A small change in phase angle can drastically change the power transfer efficiency, which makes taking efficiency measurements difficult. The difference between a measurement of 80° and a measurement of 77.6° varied slightly on the oscilloscope. At a D of 40 mm, the measured phase angle was 80°, and the power transferred efficiency was measured at 73 percent. If we change the phase angle to the value measured at 35 mm (77.6°), the power transfer efficiency is 59.8 percent. This efficiency fits in with the other measured data, and the measured data plot would

decrease at all values of *D*. Therefore, the discrepancy may be due to error in measuring the phase angle at this distance.

The differences in power transfer efficiencies between the calculated and measured values shown in Figure 23 can be attributed to losses within the system. One such loss is heating losses due to the current flowing through the 18 gauge wire that make up the composition of the coils, but the biggest loss to the IPT system can be attributed to magnetic flux coupling between the coils. When the coils were close together, the flux coupling between the coils was high, and the measured efficiency values were close to the calculated values. When the distance between the coils increased, flux coupling between the coils decreased, causing a drop in power transferred.

Another cause for a decrease in magnetic flux coupling is due to coil misalignment [21]. At every distance increment, the coils were checked visually to minimize misalignment between the coils, but coil misalignment could still be a small contributing factor to the difference in efficiencies. We further tried to minimize the effects of coil misalignments by using a series-series compensation topology as discussed in [21].

4. Measured Power Transfer Efficiency with Ferrite Tiles

As discussed in Section IV.A.3, power transfer efficiency greatly decreased as the distance between the coils increased due less magnetic flux coupling. A way to guide the magnetic flux and increase flux coupling is to add a ferrite surface behind the receiving coil. Six ferrite tiles were attached to a plastic board, and the board was then placed behind the receiving coil, as shown in Figure 24. The number of available tiles was limited, which forced the irregular arrangement. The placement of the ferrite board behind the receiving coil was suggested by SSC Pacific. The value of μ_r was not available from the manufacture, but based on the fact that the tiles are made from a nickel-zinc material, a reasonable value is $\mu_r \approx 20.0$.

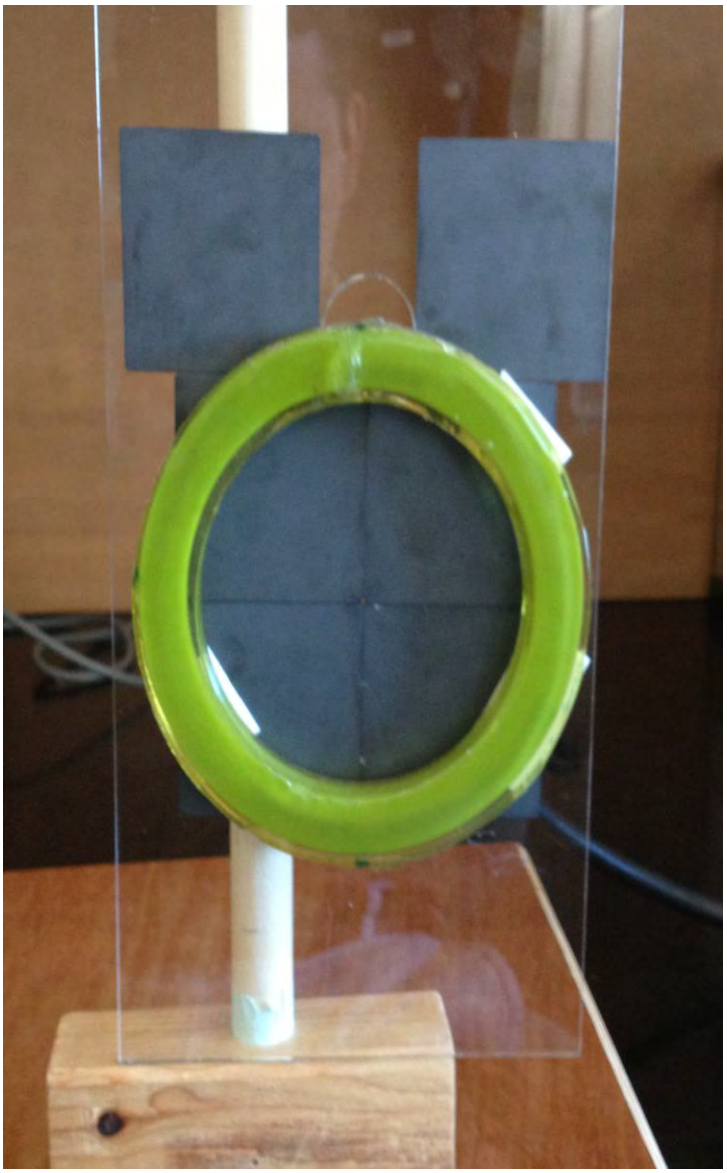

Figure 24. Photograph of the ferrite board behind the receiving coil.

The effect of a ferrite plate is illustrated in the plots shown in Figure 25. In Figure 25(a), the magnetic field of a magnet is shown. The magnet, which is equivalent to a current loop, represents the transmitting coil. The rectangle on the right is the location of the ferrite tile and is assigned $\mu_r = 1.0$. A relative magnetic permeability of 1.0 represents an IPT system without ferrite tiles. In Figure 25(b), the rectangle on the right is assigned $\mu_r = 20.0$, which represents an IPT system with ferrite tiles. The concentration of the magnetic field is apparent when comparing Figure 25(a) and Figure

25(b). This shows that the ferrite tiles help concentrate the magnetic flux in an IPT system. The plots in Figure 25 were created using Vizimag 3.18.

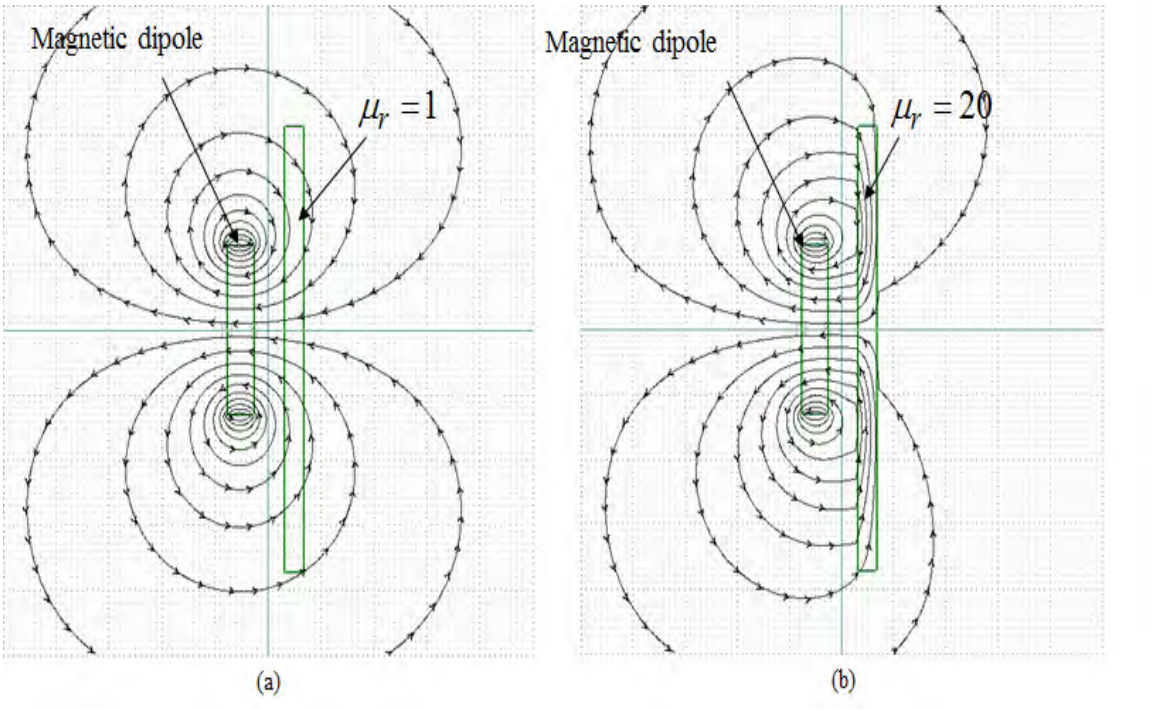

Figure 25. Plot of the magnetic flux (a) without ferrite tile and (b) with ferrite tile.

Using the system setup shown in Figure 26, we took voltage and current measurements and measured system efficiency was determined with the ferrite tiles. The efficiency results of the IPT system with the ferrites were compared to the theoretical efficiencies as shown in Table 2 and the measured efficiencies without the ferrites as shown in Figure 23. The results were plotted and shown in Figure 27. The ferrite tiles did allow for more magnetic flux coupling and raised efficiency at all measured air gaps. The benefit of the ferrite tiles was most evident at larger distances. At an air gap of 150 mm, the power transfer efficiency improved from 1.0 percent without the ferrite tiles to 16.5 percent with the ferrite tiles. The current and voltage data can be found in Appendix D.

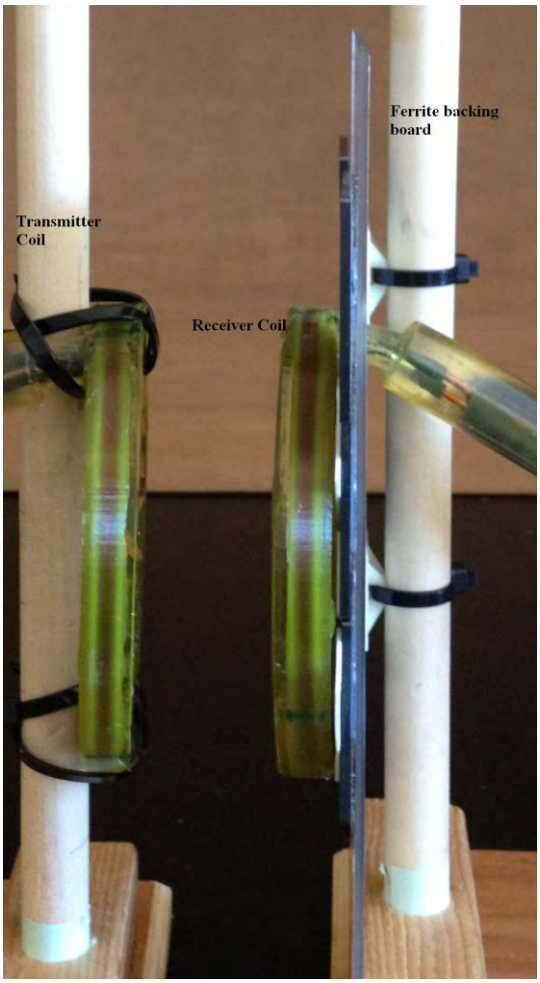

Figure 26. Setup of the transmitter coil and receiver coil with a ferrite backing plate.

As noted previously, system efficiency should continue to decrease monotonically as the distance between the coils increases, as shown by the red line in Figure 27, but the measured efficiency with the ferrite tiles did not continue to decrease as the coil distance increased, as shown by the blue line in Figure 27. At 30 mm, 55 mm, 75 mm, and 100 mm the efficiency increased rather than decreased. It was also noted that at 60 mm and 70 mm power transfer efficiency is significantly lower than expected. A possible reason for the discrepancy can be attributed to reading the phase angle, as discussed previously in Section IV.A.3. Another possible source of discrepancy may be due to the irregular arrangement of the ferrite tiles. The irregular arrangement of the tiles may cause a non-symmetrical magnetic field distribution and be a source contributing to the irregular measurements. If we exclude these points, the measured efficiencies with the ferrites

would decrease similar to the calculated efficiencies. The difference between the measured efficiencies with ferrite and the calculated efficiencies can be attributed to the losses previously discussed in this chapter.

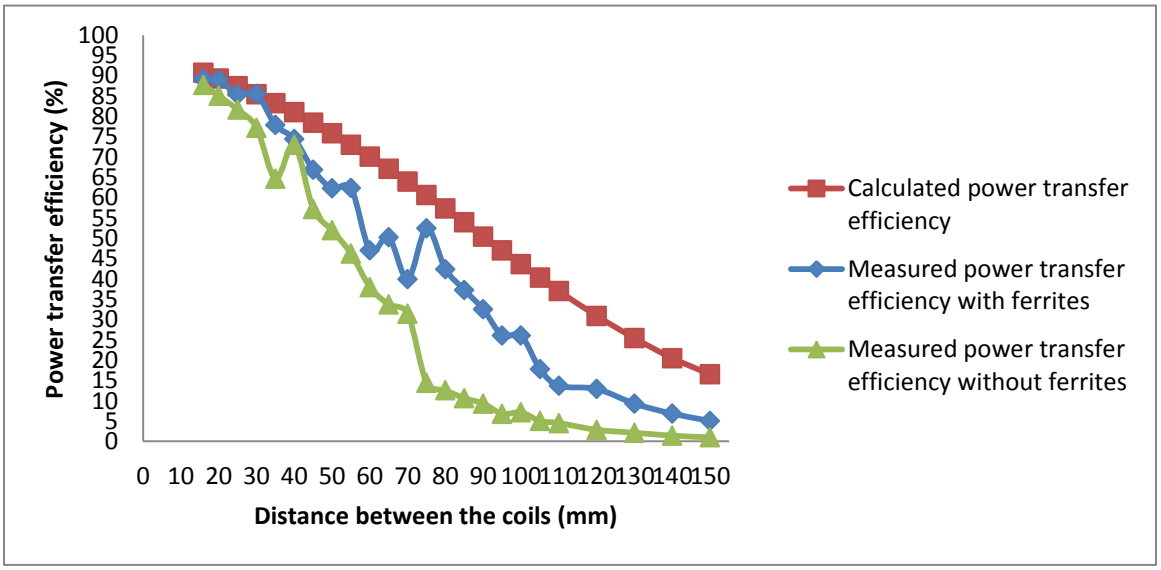

Figure 27. Comparison of the measured power transfer efficiency for the three test configurations as a function of distance between the transmitter and receiver coils.

5. Measured power transfer efficiency with the receiving coil inside an aluminum AUV hull

We have established the baseline power transfer efficiency of two coils without ferrite tiles and with ferrite tiles. Next we modified the IPT system setup to include an aluminum AUV hull. The aluminum hull is similar to the one used by a REMUS AUV. The IPT system was setup similar to what would be used at a REMUS docking station. The system was setup as shown in Figure 28 with the receiving coil placed inside the AUV hull.

Figure 28. Setup of the transmitting coil and receiving coil with backing plate inside an AUV hull.

The AUV hull has two cutouts. The first hull cutout was sized to match the circumference of the receiving coil, as shown in Figure 29. The second hull opening was made to allow for the receiver coil wires to pass through the hull and into the battery section of a REMUS AUV. With the backing plate attached, the receiving coil only extends a few millimeters past the AUV hull, as shown in Figure 28. Since the receiving

coil only extends a few millimeters past the hull, the water flow characteristics of the hull moving through seawater should not be greatly affected.

Figure 29. The receiving coil and ferrite backing plate inside of the AUV hull.

Due to the hull shape, the closest measurement that could be taken was at 30 mm. Voltage and current measurements were taken, and measured efficiency was plotted as shown in Figure 30. The measured efficiency with the AUV hull was never better than the measured efficiencies of the system without the hull. The measured data stops at 95 mm because the power transfer efficiency of the system fell below 1 percent at 95 mm. The reason for the poor efficiency can be attributed to the aluminum hull.

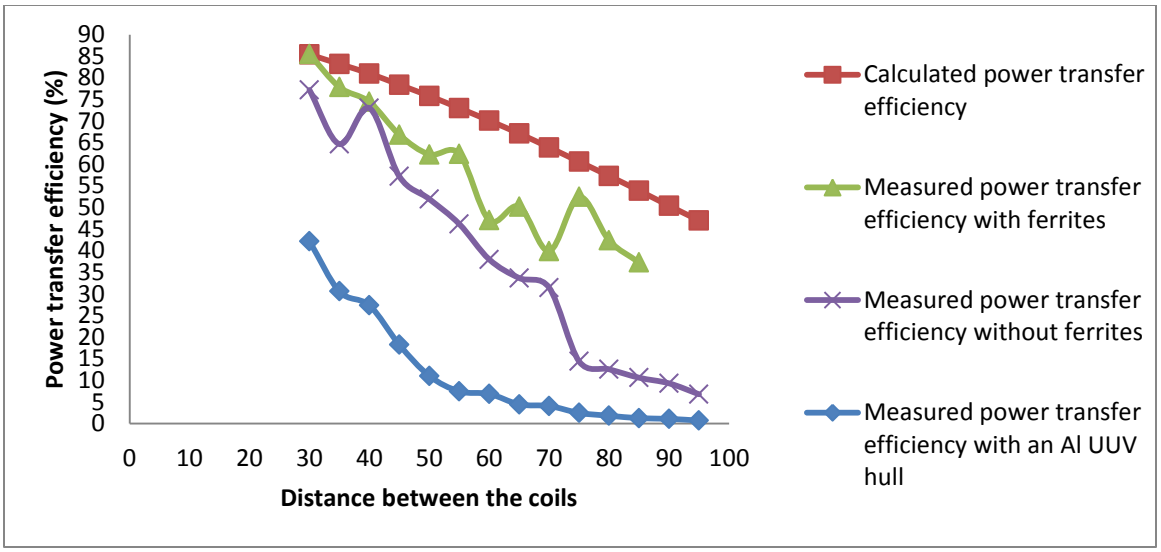

Figure 30. Power transfer efficiency of the IPT system with the receiving coil and ferrite backing material inside of the AUV hull.

Since the receiving coil was inside the aluminum hull, the aluminum hull acted as an attenuator due to eddy currents generated on the hull. Since the receiving coil was not fully encased by the aluminum hull, some free space magnetic coupling occurred between the coils but became weaker as distance between the coils increased. The voltage and current data can be found in Appendix E.

6. Summary

Power transfer efficiency was greatly improved with the addition of a ferrite tiles behind the receiving coil. An increase of 15.5 percent efficiency was achieved with an air gap of 150 mm. The increase in efficiency was due to the increase magnetic flux density caused by the ferrites. An aluminum AUV hull was introduced to the IPT system and efficiency greatly decreased. The cause of the decrease was due to the aluminum hull acting like a shield and causing less magnetic coupling to occur between the coils, as shown in Figure 30.

V. METHODS TO IMPROVE POWER TRANSFER EFFICIENCY

A. METHODS THAT DO NOT REQUIRE MODIFICATION OF THE COILS

1. Change the Compensation Topology

As discussed in Chapter IV, a simple way to improve power transfer efficiency is to add ferrite tiles to the IPT system. Another simple way that would improve efficiency is to change the compensation topology. A better topology for this IPT system is a series-parallel topology, as shown in Figure 8. In a few studies, [5], [10], and [11], a series-parallel topology was shown to work best for battery charging applications. The disadvantage in using a series-parallel topology is that the tolerance to coil misalignment provided by a series-series topology is lost.

2. Increase Frequency

From Eq. (36), increasing the operational frequency from 100 kHz to 300 kHz raises efficiency from 90.7 percent to 96.8 percent at an air gap of 16 mm. When the coils are in air, increasing the frequency improves efficiency because of the increased magnetic coupling between the coils; but when the coils are placed in seawater, the increase in frequency causea a power loss due to the conductivity of the seawater [22]. As noted in [3], for the coils used in this research, when the frequency is increased above 100 kHz, the water resistance increases and causes a decrease in coupling coefficient and efficiency.

3. Increase the Number of Coils

It has been shown in [23] and [24] that, if we use the four-coil IPT system as shown in Figure 31, we can achieve a power transfer efficiency greater than that of a two coil system. Despite improving system efficiency, a four-coil system is impracticable for this AUV docking platform design.

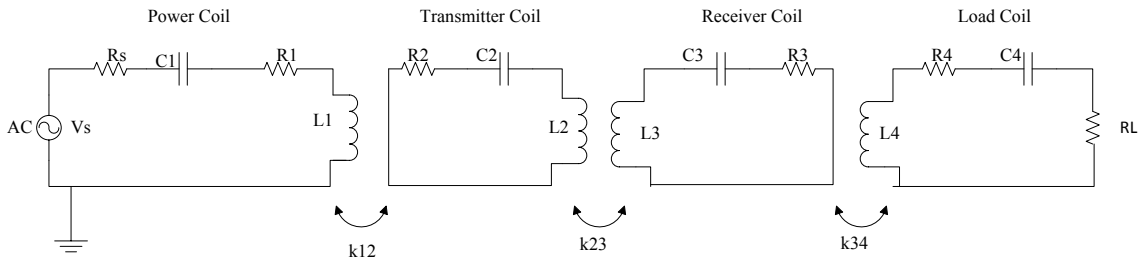

Figure 31. Circuit model of a four-coil IPT system (from [23]).

4. Change the Hull Material

As shown in Figure 30, power transfer efficiency decreased when the receiving coil was placed within the aluminum hull form. Therefore, by changing the hull material from aluminum to a hull material that does not attenuate the magnetic flux we can increase efficiency. We would not necessarily need to change the hull composition of the entire AUV but only in the section containing the receiving coil.

5. Increase the Distance the Receiver Coil Extends Past the AUV Hull

As shown in Figure 29, the receiving coil extends only a few millimeters past the AUV hull. If we extended the coil out past the AUV hull, we could possibly decrease the effects of shielding due the hull, but increasing the distance the receiving coil extends past the AUV hull affects the way the AUV moves through the water. More analysis is needed to determine if this solution would be useful in increasing system efficiency and yet not cause a significant change in the underwater characteristics of the AUV.

B. METHODS THAT REQUIRE MODIFICATION OF THE COIL

1. Improve the Coil's Quality Factor

The methods discussed in Section V.A focused on techniques that did not involve changing the coil's properties; but if we are allowed to change the coils, then there are several more ways to improve efficiency. As shown in Eq. (37), efficiency can be improved by increasing the Q of the coils, increasing the k between the coils, or by increasing both Q and k. The simplest way to improve Q is to increase the number turns of the coil while reducing the winding separation between the coils [19]. The downside

of reducing the winding separation is that it increases the parasitic capacitance of the coils and lowers the self-resonance frequency of the coils, causing an upper limit to the operating frequency [19]. If this upper limit is below 100 kHz, then this would be a viable option to increase efficiency.

2. Improve the Coil's Coupling Coefficient

The three common coil shapes used in IPT are circular, square, and rectangular. Each coil shape was used in [19] to determine which shape has the biggest influence on increasing *k*. It was determined for a given area of a coil, that *k* was a little larger for the circular coil than the rectangular and square coils. It was presumed that the decrease in *k* for the square shape and rectangular shape coils can be attributed to the distortion of the magnetic field around the corners of the square and rectangle [19]. Overall, differences in *k* between the circular coil and the square and rectangular coils are small. Changing the shape of coils contributes little to improving power transfer efficiency, but it was shown in [19] that increasing the area of the receiving coil produces a higher value of *k*. Therefore, we should maximize the area of the receiving coil that can fit in the AUV hull.

There are two more ways to increase *k*. The first is to decrease the inner radius of the coils [19]. The inner radius is defined as the radius from the center of the coil to the inner wall of the coil. The second way to improve *k* is to design the transmitting coil to be larger than the receiving coil [19]. By increasing the size of the transmitting coil, we increase the magnetic flux between the coils.

3. Change the Coil Material

The coils used for this research were comprised of 18 gauge (AWG) wire. These coils could be improved by substituting the 18 gauge wire with Litz wire. Litz wire is made up of a multiple twisted strands of wire of equal length and each strand is electrically isolated from the others. The benefit of Litz wire is that it reduces losses generated in the coil. By decreasing the losses in the coil, we can increase the amount of power transferred to the load.

C. SUMMARY

As discussed in Section V.A and V.B, there are several methods we can use to increase the power transfer efficiency. The methods were placed into two categories. The first category involved methods that do not require modification to the coils, and the second category required modifications to the coils. In the first category we determined that the easiest way to increase efficiency was to increase the operating frequency of the system, but increasing frequency actually decreases efficiency when the coils are placed in seawater. Another technique is to change the compensation topology from series-series to series-parallel, a topology used in many battery charging applications. The next technique discussed was the use a four-coil IPT system, but such a system is impractical with the current AUV docking platform. Another alternative method required the receiving coil to be extended past the AUV hull, but by extending the coil we possibly change the underwater profile of the AUV. Finally, if we simply change the hull material around the receiving coil, we can increase efficiency to the blue line values shown in Figure 27.

In the second category, we looked at ways to increase the Q and k of the system by changing how the coils were made. We discussed that increasing the number of turns and reducing the winding separation increases Q. We can increase k by optimizing the receiving coil radius to the AUV hull, reducing the inner radius of the coils and building a transmitting coil larger than the receiving coil. The final technique explored was to change the composition of the coils from 18 gauge wire to Litz wire.

VI. SUMMARY, CONCLUSION, AND FUTURE WORK

A. SUMMARY

In this report we demonstrated that wireless power transfer, specifically inductive power transfer, can be a viable way to charge a REMUS AUV underwater. By using IPT, we can eliminate the need for electrical contacts within the docking station and also eliminate the need to construct multiple docking stations to fit every type of AUV. It was also shown that ferrite plates increase power transfer efficiency and that the aluminum AUV hull acted to attenuate the magnetic flux causing a decrease in efficiency, as shown in Figure 30, but there are several simple methods to increase system efficiency, as discussed in Chapter V.

B. CONCLUSION

IPT can be a viable method to charge an AUV in situ, as shown by the data plotted in Figure 30, but some changes to this IPT system are needed to increase power transfer efficiency. In Chapter V, we discussed several easy methods to raise efficiency. By using some of these methods, we can raise the efficiency of our IPT system and demonstrate that IPT is a viable option to charge a REMUS AUV. We can leverage this information to create a single docking station that could accommodate all types of AUV hulls. The shift from purchasing multiple docking stations to a single docking station will save the USN money. We recommend continuing work in IPT focusing on the improvement methods discussed in Chapter V.

C. AREAS OF FUTURE WORK

In this thesis several ways to improve power transfer efficiency were discussed. Future work could involve incorporating some or all of the improvement techniques. We recommend optimizing the receiver coil to the area available on the AUV, changing the hull material, changing the coil composition to Litz wire and creating a larger transmitter coil to increase efficiency. Once these changes are made, we can compare the measured efficiency results to the efficiency results in this thesis.

Another area of future work is to study a four-coil IPT system. We could determine how much a four coil system improves efficiency and then determine if we could implement a four-coil IPT into a new or existing AUV docking system.

A series-series compensation topology allows for greater misalignment tolerance between the coils while still allowing for high power transfer efficiency; however, there is a question as to how much angular misalignment the system can tolerate before efficiency drops below what is necessary to charge the AUV efficiently. The results of this area of future work can be compared to similar work conducted using rectangular coils [5], [21] and other circular coils [25], [26].

In this thesis we studied an IPT system that consists of only compensation capacitors, coils and a load. However, a complete system would also have variable frequency controllers and a frequency controlled power supply. A future area of work is to study how an IPT system with these extra components operate at the required frequency and within the bifurcation region. The results can be compared to other studies performed [27]–[29].

APPENDIX A. DERVIATION OF MATCHED LOAD RESISTANCE

From Eq. (35)

$$\eta = \frac{R_L(\omega_0 M)^2}{R_1(R_2 + R_L)^2 + (\omega_0 M)^2(R_2 + R_L)}. \tag{A1}$$

Take the derivative with respect to R_L and set the result to zero to get

$$\begin{aligned} 0 &= (\omega M)^2[R_1R_2^2 + 2R_1R_2R_L + (\omega M)^2 R_2 + (\omega M)^2 R_L]^{-1} \\ &-[R_1R_2^2 + 2R_1R_2R_L + R_1R_L^2 + (\omega M)R_2 + (\omega M)^2 R_L]^{-2}([R_L(\omega M)^2]\,[2R_1R_2 + 2R_1R_L + (\omega M)^2]). \end{aligned} \tag{A2}$$

Simplifying the result

$$R_L(2R_1R_2 + 2R_1R_L + (\omega M)^2) = R_1R_2^2 + 2R_1R_2R_L + R_1R_L^2 + R_2(\omega M)^2 + R_L(\omega M)^2, \tag{A3}$$

and solving for R_L, which becomes $R_{L,matched}$, we get

$$R_L^2 = R_2^2 + \frac{R_2}{R_1}(\omega M)^2 \tag{A4}$$

$$R_{L,matched} = \sqrt{R_2^2 + (\omega M)^2 \frac{R_2}{R_1}}. \tag{A5}$$

THIS PAGE INTENTIONALLY LEFT BLANK

APPENDIX B. MATLAB SCRIPT FILE

This appendix contains the Matlab script that calculates mutual inductance and power transfer efficiency at different air gaps.

```
clc
clear
% exact M, Rl_matched and efficiency

clear
format long
format compact
b=0.06; %radius of the receiver coil
a=0.06; %radius of the transmitter coil
Nt=20; %number of turns of the transmitter coil
Nr=20; %number of turns of the receiver coil
D=[0.016 0.020 0.025 0.030 0.035 0.040 0.045 0.050 0.055 0.06 0.065
0.07 0.075 0.080 0.085 0.090 0.095 0.1 0.105 0.11 0.12 0.13 0.14 0.15
0.16 0.17 0.18 0.19 0.20 0.21 0.23 0.25];
%distance between the transmitter and receiver coils
mu0=4*pi*1e-7;
mur=1; %relative permeability of air.  Permeability of SW is close
enough to air.
mu=mu0*mur;
% use elliptic formulas
for i=1:length(D)
A=(a^2+b^2+D(i)^2)/b^2/a^2;
B=2/a/b;
beta=sqrt(2*B/(A+B));
K=mfun('EllipticK',beta);%first order elliptical integral
E=mfun('EllipticE',beta);%second order elliptical integral
% exact formula
M(i)=Nt*Nr*2*mu*sqrt(A+B)/B*((1-beta^2/2)*K-E);%equation for mutual
induction
end

f=100e3; %frequency of operation
omega=2*pi*f;
R1=1.34; %internal resistance of the transmitter coil
R2=1.32; %internal resistance of the receiver coil
Rl_matched=sqrt(R2^2+omega^2.*M.^2*(R2/R1)); %matched load resistance
equation varies with frequency and M
eta=((omega^2.*M.^2.*Rl_matched)./(R1.*(R2+Rl_matched).^2+omega^2.*M.^2
.*(R2+Rl_matched)))*100;
%efficiency equation based on distance between transmitter and receiver
%coil

disp('  D           M             Rl       eta')
for i=1:length(D)
    disp([num2str(D(i)),'     ',num2str(M(i)),'
',num2str(Rl_matched(i)),'     ',num2str(eta(i))])
end
```

```
figure(1)
plot(D,M,'-r')
xlabel('Distance between transmitter and receiver coils (m)')
ylabel('Mutual inductance (H)')
title('Mutual inductance (M) as a function of the distance between
transmitter and receiver coils')

figure (2)
plot(D,eta,'-r')
xlabel('Distance between transmitter and receiver coils (m)')
ylabel('Power transfer efficiency (%)')
title('Power transfer efficiency as a function of the distance between
transmitter and reciever coils')

figure (3)
plot(D,Rl_matched,'-r')
xlabel('Distance between transmitter and receiver coils (m)')
ylabel('Rl_matched as a function of the distance between transmitter
and receiver coils')
```

APPENDIX C. MEASURED DATA IN AIR AND WITHOUT FERRITES

Table C1. Raw data for coils in air, no ferrite tiles.

Distance between the transmitter and receiver coils (mm)	Transmitter voltage (V)	Transmitter current (A rms)	Load voltage (V rms)	Load current (I rms)	Phase angle	Efficiency
16	25.00	0.321733585	6.505	0.236880772	72.00	87.6796616
20	25.20	0.325622673	5.515	0.261629509	73.00	85.0610641
25	26.00	0.346482323	5.091	0.261629509	75.16	81.6432286
30	27.40	0.374766594	4.667	0.254558441	77.76	77.1737454
35	28.00	0.38890873	3.818	0.276478751	77.76	64.6694803
40	23.00	0.300520382	2.970	0.2085965	80.00	72.9935205
45	26.60	0.374766594	2.828	0.247487373	80.00	57.1873931
50	26.60	0.381837662	2.546	0.254558441	80.00	51.9588314
55	26.60	0.381837662	2.263	0.254558441	80.00	46.1856279
60	25.80	0.360624458	1.980	0.219203102	80.00	37.9891532
65	26.00	0.374766594	1.838	0.219203102	80.00	33.6833745
70	26.20	0.367695526	1.697	0.219203102	80.00	31.4483649
75	26.70	0.381837662	0.962	0.187383297	80.00	14.3949291
80	26.60	0.381837662	0.905	0.173241161	80.00	12.5727543
85	26.60	0.381837662	0.750	0.176776695	80.00	10.6242981
90	26.80	0.374766594	0.707	0.16263456	80.00	9.32495924
95	27.00	0.381837662	0.608	0.141421356	80.00	6.79361127
100	24.60	0.346482323	0.481	0.155563492	80.00	7.14710523
105	24.40	0.346482323	0.410	0.127279221	80.00	5.0285684
110	24.60	0.346482323	0.382	0.123743687	80.00	4.51471554
120	24.80	0.346482323	0.318	0.094752309	80.00	2.85758608
130	24.60	0.353553391	0.233	0.097580736	80.00	2.13214966
140	25.00	0.353553391	0.187	0.082024387	80.00	1.4108527
150	25.00	0.360624458	0.156	0.070710678	80.00	0.9936702

THIS PAGE INTENTIONALLY LEFT BLANK

APPENDIX D. MEASURED DATA IN AIR WITH FERRITES

Table D1. Raw data for coils in air, with ferrite tiles.

Distance between the transmitter and receiver coils (mm)	Transmitter voltage (V)	Transmitter current (A rms)	Load voltage (V rms)	Load current (I rms)	Phase angle	Efficiency
16	25.00	0.296984848	8.061	0.332340187	55.08	89.143445
20	29.00	0.367695526	7.354	0.346482323	67.68	88.980947
25	25.80	0.346482323	5.374	0.261983062	74.88	85.390453
30	25.40	0.346482323	4.667	0.297338401	74.88	85.487662
35	26.00	0.353553391	4.243	0.311126984	74.88	77.854528
40	26.00	0.353553391	3.677	0.311126984	76.32	74.41892
45	26.20	0.360624458	3.394	0.311126984	76.32	66.833337
50	26.20	0.360624458	2.970	0.296984848	77.76	62.269688
55	23.00	0.318198052	2.121	0.247487373	80.64	62.377671
60	21.60	0.311126984	1.584	0.194454365	82.08	47.038739
65	19.80	0.247487373	1.329	0.180312229	82.08	50.204908
70	20.20	0.254558441	1.131	0.176776695	82.08	39.919722
75	20.20	0.254558441	0.948	0.176776695	84.96	52.437654
80	20.20	0.258093975	0.863	0.159099026	84.96	42.378974
85	20.60	0.261629509	0.735	0.169705627	84.96	37.275884
90	20.60	0.265165043	0.693	0.159099026	84.96	32.490951
95	21.00	0.265165043	0.622	0.14495689	84.96	26.075839
100	18.80	0.240416306	0.481	0.152027958	84.96	26.03532
105	19.00	0.24395184	0.403	0.127279221	84.96	17.816688
110	19.00	0.247487373	0.368	0.108894444	84.96	13.707389
120	19.40	0.247487373	0.304	0.090509668	86.40	12.909653
130	19.40	0.247487373	0.212	0.093338095	86.40	9.2881952
140	19.40	0.247487373	0.184	0.079195959	86.40	6.8301072
150	19.40	0.247487373	0.156	0.069296465	86.40	5.0569063

THIS PAGE INTENTIONALLY LEFT BLANK

APPENDIX E. MEASURED DATA WITH THE RECEIVER COIL INSIDE THE AUV HULL

Table E1. Raw data for coils in air with receiver coil placed inside the AUV hull.

Distance between the transmitter and receiver coils (mm)	Transmitter voltage (V)	Transmitter current (A rms)	Load voltage (V rms)	Load current (I rms)	Phase angle	Efficiency
30	25.40	0.342946789	1.697	0.09617	86.40	42.196907
35	26.40	0.38890873	1.273	0.08768	87.12	30.594307
40	21.80	0.325269119	0.778	0.06647	87.84	27.357598
45	22.20	0.325269119	0.636	0.05515	87.84	18.238876
50	22.60	0.332340187	0.467	0.04738	87.84	11.04547
55	22.60	0.332340187	0.346	0.04313	87.84	7.4660583
60	20.60	0.296984848	0.311	0.03606	87.84	6.8814205
65	20.60	0.272236111	0.209	0.03182	87.84	4.4560292
70	20.60	0.272236111	0.156	0.02616	88.56	4.084156
75	20.80	0.272236111	0.112	0.02227	88.56	2.4731442
80	20.80	0.272236111	0.095	0.01945	88.56	1.8311305
85	20.80	0.272236111	0.072	0.01768	88.56	1.2671323
90	21.00	0.272236111	0.066	0.01697	88.56	1.1103629
95	21.00	0.272236111	0.054	0.01344	88.56	0.710711

THIS PAGE INTENTIONALLY LEFT BLANK

LIST OF REFERENCES

[1] Woods Hole Oceanographic Institution (WHOI), "AUV docking station integration with NPS Monterey Inner Shelf Observatory (MISO)," SPAWAR, San Diego, CA, Status Report Jun. 2013.

[2] R. Stokey, M. Purcell, N. Forrester, T. Austin, R. Goldsborough, B. Allen and C. Alt, "A docking system for REMUS, an autonomous underwater vehicle," in *IEEE Conf. OCEANS*, Halifax, Canada, pp. 1132–1136, 1997.

[3] V. Bana, G. Anderson, L. Xu, D. Rodriguez, A. Phipps and J. Rockway, "Characterization of coupled coils in seawater for wireless power transfer," SPAWAR, San Diego, CA, Tech. Rep. 2026, 2013.

[4] N. Shinohara, "Power without wires," IEEE Microwave, vol. 12, no. 7, pp. S64–S73, Dec. 2011.

[5] J. Sallan, A. Llombart and J. Sanz, "Optimal design of ICPT systems applied to electric vehicle battery charge," IEEE Trans. Ind. Electron., vol. 56, no. 6, pp. 2140–2149, Jun. 2009.

[6] V. Bana, private communication, August 2013.

[7] W. C. Brown, "The history of power transmission by radio waves," IEEE Trans. Microw. Theory Tech., MTT-32, no. 9, pp. 1230–1242, Sept. 1984.

[8] F. Ulaby, "Maxwell's equations for time-varying fields," in *Fundamentals of applied electromagnetics*, 5th ed. Upper Saddle River: Pearson Prentice Hall, pp. 255–270, 2007.

[9] B. Knuteson, G. Stephans, J. Belcher, J. Joannopolus, M. Feld and P. Dourmashkin. 8.02T Electricity and magnetism, Spring 2005 [Online]. Available: http://www.web.mit.edu/viz/EM/visualizations/coursenotes/modules/guide11.pdf

[10] O. H. Stielau and G. A. Covic, "Design of loosely coupled inductive power transfer systems," in *Int. Conf. on Power System Technology*, Perth, Australia, pp. 85–90, 2000.

[11] R. Laouamer, M. Brunello, J. Ferrieux, O. Normand and N. Buchheit, "A multi-resonant converter for non-contact charging with electromagnetic coupling," in *23rd Int. Conf. on Industrial Electronics, Control and Instrumentation*, New Orleans, LA, pp. 792–797, 1997.

[12] J. L. Villa, A. Llombart, J. Sanz and J. Sallan, "Practical development of a 5 kW ICPT system SS compensated with a large air gap," in *IEEE Int. Symp. on Industrial Electronics*, Vigo, Spain, pp. 1219–1223, 2007.

[13] T. McGinnis, C. Henze and K. Conroy, “Inductive power system for autonomous underwater vehicles,” in *IEEE Conf. OCEANS*, Vancouver, Canada, pp. 1219–1223, 2007.

[14] B. J. Heeres, D. Novotny, D. Divan and R. Lorenz, “Contactless underwater power delivery,” in *25th Annu. Power Electronics Specialists Conferenc*e, Taipei, Taiwan, pp. 418–423, 1994.

[15] B. S. Lee and K. H. Han, “Modeling and analysis of IPT system used for PRT,” in *Eighth Int. Conf. on Electrical Machines and Systems*, Nanjing, China, pp. 839–842, 2005.

[16] Q. Wang and H. Li, “Research on the wireless power transmission system based on coupled magnetic resonances,” in *Int. Conf. on Electronics, Communications and Control*, Ningbo, China, pp. 2255–2258, 2011.

[17] W. Fu, B. Zhang, D. Qiu and W. Wang, “Analysis of transmission mechanism and efficiency of resonance coupling wireless energy transfer system,” in Int. Conf. on Electrical Machines and Systems, Wuhan, China, pp. 2163–2168, 2008.

[18] J. O. Mur-Miranda, G. Fanti, Y. Feng, K. Omanakuttan, R. Ongie, A. Setjoadi and N. Sharpe, “Wireless power transfer using weakly coupled magnetostatic resonators,” in *IEEE Energy Conversion Congress and Exposition*, Atlanta, GA, pp. 4179–4186, 2010.

[19] R. Bosshard, J. Muhlethaler, J. Kolar and I. Stevanovic, “Optimized magnetic design for inductive power transfer coils,” in *Twenty-Eighth Annul, IEEE Applied Power Electronics Conference and Exposition*, Long Beach, CA, pp. 1812–1819, 2013.

[20] J. Garnica, J. Casanova and J. Lin, “High efficiency midrange wireless power transfer system,” in *IEEE MTT-S Int. Microwave Workshop Series on Innovative Wireless Power Transmission: Technologies, Systems, and Applications*, Kyoto, Japan, pp. 73–76, 2011.

[21] J. Villa, J. Sallan, J. Osorio and A. Llombart, “High-misalignment tolerant compensation topology for ICPT systems,” *IEEE Trans. Ind. Electron.*, vol. 59, no. 2, pp. 945–951, Feb. 2012.

[22] J. Zhou, D. Li and Y. Chen, “Frequency selection of an inductive contactless power transmission system for ocean observing,” *Ocean Engineering*, vol. 60, no. 1, pp. 175–185, 2013.

[23] M. Kiani and M. Ghovanloo, “A figure-of-merit for designing high-performance inductive power transmission links,” *IEEE Trans. Ind. Electron*., vol. 60, no. 11, pp. 5292–5305, 2013.

[24] H. Hoang and F. Bien. (2012, Jan. 25). Maximizing efficiency of electromagnetic resonance wireless power transmission systems with adaptive circuits [Online]. Available: http://www.intechopen.com/books/wireless

[25] B. W. Flynn and K. Fotopoulou, "Wireless power transfer in loosely coupled inductive links with lateral and angular misalignment," *IEEE Microwave*, vol. 13, no. 2, pp. 48–54, 2013

[26] J. Wang, J. Li, S. Ho, W. Fu, Y. Li, H. Yu and M. Sun, "Lateral and angular misalignment analysis of a new PCB circular spiral resonant wireless charger," *IEEE Trans. Magn*., vol. 48, no. 11, pp. 4522–4525, 2012.

[27] C.S. Wang, G. Covic and O. Stielau, "Power transfer capability and bifurcation phenomena of loosely coupled inductive power transfer systems," *IEEE Trans. Ind. Electron*., vol. 51, no. 1, pp. 148–157, 2004.

[28] J. T. Boys and A. W. Green, "Stability and control of inductively power transfer systems," *Proc. IEEE Electric Power Applications*, vol. 147, no. 1, pp. 37–43, 2000.

[29] C. S. Wang, G. Covic and O. Stielau, "General stability criterions for zero phase angle controlled loosely coupled inductive power transfer systems," in *27th Annu. Conf. of the IEEE Industrial Electronics Society*, Denver, CO, pp. 1049–1054, 2001.

THIS PAGE INTENTIONALLY LEFT BLANK

INITIAL DISTRIBUTION LIST

1. Defense Technical Information Center
   Ft. Belvoir, Virginia

2. Dudley Knox Library
   Naval Postgraduate School
   Monterey, California